MASARYKOVA UNIVERZITA

PŘÍRODOVĚDECKÁ FAKULTA

Telomery v mutantních liniích Physcomitrium patens s aktivovaným mechanismem alternativního prodlužování telomer

Diplomová práce

ANNA VÁVRA

Vedoucí práce: doc. Mgr. Miloslava Fojtová, CSc.

Národní centrum pro výzkum biomolekul
Program Biochemie

Brno 2026

MUNI
SCI

Bibliografický záznam

Autor: Anna Vávra
Přírodovědecká fakulta
Masarykova univerzita
Národní centrum pro výzkum biomolekul

Název práce: Telomery v mutantních liniích Physcomitrium patens s aktivovaným mechanismem alternativního prodlužování telomer

Studijní program: Biochemie

Studijní obor: Genomika a proteomika

Vedoucí práce: doc. Mgr. Miloslava Fojtová, CSc.

Rok: 2026

Počet stran: 108

Klíčová slova: Physcomitrium patens, telomery, telomeráza, alternativní prodlužování telomer, telomerázová RNA

Bibliographic record

Author: Anna Vávra
Faculty of Science
Masaryk University
National Centre for Biomolecular Research

Title of Thesis: Telomeres in Physcomitrium patens mutant lines with activated alternative telomere elongation mechanism

Degree Programme: Biochemistry

Field of Study: Genomics and proteomics

Supervisor: doc. Mgr. Miloslava Fojtová, CSc.

Year: 2026

Number of Pages: 108

Keywords: Physcomitrium patens, telomeres, telomerase, alternative lengthening of telomeres, telomerase RNA

Abstrakt

Telomery jsou nukleoproteinové struktury, které hrají zásadní roli v ochraně konců lineární chromozomů tím, že (1) kompenzují nekompletní replikaci konců chromozomů vedoucí k jejich zkracování a (2) odlišují konce chromozomů od dvouvláknových DNA zlomů, a tím předcházejí jejich opravě a fúzi. Telomery jsou zkracovány s každým buněčným cyklem, a proto jejich délka slouží jako kontrolní mechanismus v savčích buňkách. Telomery jsou prodlužovány primárně nukleoproteinovým enzymem telomerázou, která se skládá ze dvou podjednotek – telomerázové reverzní transkriptázy (TERT) a telomerázové RNA (TR). V některých případech mohou být telomery prodlužovány alternativně, pomocí na telomeráze-nezávislého mechanismu, označovaného jako alternativní prodlužování telomer (alternative lengthening of telomeres; ALT). ALT byl identifikován např. v rakovinných buňkách nebo v mutantních rostlinách – mutantu *Arabidopsis thaliana* s nefunkčním TERT nebo TR mutantu *Physcomitrium patens*.

Tato práce se zabývá charakterizací telomer dlouhodobě přežívajících mutantních linií mechu *P. patens* s aktivovaným ALT mechanismem (*pptr*). Tyto knock-out mutanty byly připraveny výměnou genu kódujícího TR za hygromycinovou kazetu. Mezi ALT znaky, které byly v rámci této práce studovány, patřily celková délka telomer i délka telomer na specifických chromozomových raméncích. Dále pak struktura telomerového chromatinu, hladina extrachromozomálních telomerových kroužků či subtelomerové sekvence vmezeřené do telomer.

Ačkoli se úspěšně nepodařilo stanovit všechny vymezené znaky ALT, bylo provedeno velké množství optimalizací metod sloužících ke studiu těchto znaků, kterých bude využito v nadcházejícím výzkumu. Mezi úspěšně popsané či ověřené znaky patřila výrazně kratší délka telomer či výrazné zvýšení hladiny subtelomerové sekvence vmezeřené do telomer u mutantních linií *P. patens* s aktivovaným ALT.

Abstract

Telomeres are a nucleoprotein structures playing a crucial role in linear chromosome ends protection. They (1) compensate incomplete replication of chromosome ends leading to their shortening, and (2) distinguish natural chromosome ends from DNA double-strand breaks (DSBs) thereby preventing their repair and fusion. Telomeres are shortened every cell cycle and therefore their length act as a control mechanism in mammalian cells. Telomeres are elongated primarily by nucleoprotein enzyme telomerase composed of two subunits – telomerase reverse transcriptase (TERT) and telomerase RNA (TR). Alternatively, telomeres can be elongated by telomerase-independent mechanism, termed alternative lengthening of telomeres (ALT). This ALT mechanism was identified, e. g., in cancer cells, or in plant mutants – *Arabidopsis thaliana* TERT mutant or *Physcomitrium patens* TR mutant.

This thesis aims to characterize telomeres in long-term surviving *P. patens* mutant line with activated ALT mechanism (*pptr*). These knock-out mutants were prepared by replacement of the gene encoding TR with hygromycin cassette. ALT features studied in this thesis include bulk telomere length, and telomere length on specific chromosome arms. Further, structure of telomere chromatin, level of an extrachromosomal telomere circles and subtelomere sequence interspaced into telomeres were studied.

Although not all delineated ALT features were identified, huge amount of method optimisation were performed. Future research will take advantages of these successful optimisations. Among the successfully identified/verified ALT markers were significantly shorter telomeres and significant increase of the level of subtelomere sequence embedded within telomeres in *P. patens* mutants with activated ALT.

MUNI
SCI

MASARYKOVA UNIVERZITA
PŘÍRODOVĚDECKÁ FAKULTA
KOTLÁŘSKÁ 2, 611 37 BRNO
IČ: 00216224
DIČ: CZ00216224

ZADÁNÍ DIPLOMOVÉ PRÁCE

Akademický rok: 2025/2026

Ústav:	Ústav biochemie
Studentka:	Bc. Anna Vávra
Program:	Biochemie
Specializace:	Genomika a Proteomika

Ředitel *ústavu* PřF MU Vám ve smyslu Studijního a zkušebního řádu MU určuje diplomovou práci s názvem:

Název práce:	Telomery v mutantních liniích Physcomitrium patens s aktivovaným mechanismem alternativního prodlužování telomer
Název práce anglicky:	Telomeres in Physcomitrium patents mutant lines with activated alternative telomere elongation mechanism
Jazyk práce:	angličtina

Oficiální zadání:
Pomocí "homology-directed repair" byly vytvořeny knock-out mutanty mechu Physcomitrium patens s nefunkční telomerázovou RNA (tr). V pilotním experimentu byly selektovány linie schopné dlouhodobého přežívání, které vykazovaly známky aktivace alternativního, tj. na enzymu telomeráze nezávislého prodlužování telomer (ALT). Analýza délek telomer v těchto liniích ukázala výrazné změny v délce a charakteru telomerově specifického hybridizačního signálu.
V rámci diplomové práce provede studentka analýzu délek telomer v dalších generacích rt mutantů. Analyzovat bude jak celkovou délku telomer metodou TRF (terminal restriction fragments), tak telomery na vybraných ramenech chromozomů (metoda PETRA, primer extension telomere repeat amplification). Dále bude studovat vlastnosti ALT telomerového chromatinu, konkrétně přítomnost jednovláknových 3' přesahů (in gel hybridizace) a strukturu chromatinu (přístupnost pro štěpení enzymem MNase). Studentka se dále pokusí o rekonstituci aktivní telomerázy v mutantních liniích, tj. opětovné vnesení kazety s genem kódujícím TR do tr mutantů.
Výsledky získané během řešení této diplomové práce budou součástí projektu, který se snaží o pochopení mechanismů umožňujících stabilizaci konců chromozomů pro dlouhodobé přežívání rostlin bez aktivního enzymu telomerázy.

Literatura:
Fajkus P et al. Evolution of plant telomerase RNAs: Farther to the past, deeper to the roots. Nucleic Acids Res 2021, 49, 7680-7694.
Goffová I et al. Roles of RAD51 and RTEL in telomere and rDNA stability in Physcomitrella patens. Plant J 2019, 98, 1090-1105.
Fojtová M et al. Telomere length dynamics in Physcomitrella patens. Plant Mol Biol 2015, 87, 591-601.
Fojtová M et al. Terminal restriction fragments (TRF) method to analyze telomere lengths. Bio-protocol 2015, 5, e1671.
Lang D et al. The Physcomitrella patens chromosome scale assembly reveals moss genome structure and evolution. Plant J 2018, 93, 515–533.

Vedoucí práce:	doc. Mgr. Miloslava Fojtová, CSc.
Datum zadání práce:	2. 10. 2024
V Brně dne:	20. 4. 2026

Bc. Anna Vávra, 2. 10. 2024
doc. Mgr. Miloslava Fojtová, CSc., 11. 2. 2026
doc. Mgr. Jan Havliš, Dr., 16. 4. 2026

Declaration

I declare that I have prepared my thesis independently under the mentorship of the thesis supervisor and using the information sources provided in the thesis.

Brno, May 12, 2026

……

Bc. Anna Vávra

Acknowledgements

I want to express my deepest gratitude to my supervisor, doc. Mgr. Miloslava Fojtová, CSc., for her unappreciated guidance, helpfulness, and advice during preparation of experimental and writing part of this thesis. Further, I would like to thanks to RNDr. Dagmar Zachová for her help with preparation and cultivation of plant material. My gratitude belongs to Marcela Holá from Institute of Experimental Botany, CAS, Prague for providing me recombinant plasmids (*TR_KO* and *Cas9*). I would like to thanks to Mgr. Petr Fajkus, Ph.D. for processing WGS data, and to Mgr. Michal Závodník, Ph.D. for measuring DNA concentration using TapeStation.

I am also very grateful to our kitchen group for lots of fun, laugh and unappreciated tips and to my beloved husband who was supporting me all the time and was there for me, when nothing worked in the lab.

Table of Contents

List of Figures 21

List of Table 23

List of Abbreviations 24

1 Introduction 27

2 Telomeres 28

2.1 Structure of telomeres 28

2.2 Telomere-associated proteins 30

3 Telomerase 33

3.1 Telomerase reverse transcriptase (TERT) 34

3.2 Telomerase RNA (TR) 35

4 Alternative Lengthening of Telomeres (ALT) 37

5 Physcomitrium patens 39

5.1.1 Life cycle 39

6 Aims of Thesis 42

7 Material and Methods 43

7.1 Material 43

7.1.1 Plant material 43

7.1.2 Plasmids 43

7.1.3 Chemicals and solutions 43

7.1.4 Primers 46

7.1.5 Enzymes 48

7.1.6 Commercial kits 48

7.1.7 Instruments 49

7.2 Methods 49

7.2.1 Cultivation of *Physcomitrium patens* 49

7.2.2 *P. patens* transformation 50

7.2.3 DNA isolation 51

7.2.4 Nucleic acids concentration and purity measurements 51
7.2.5 Nucleic acids agarose gel electrophoresis 52
7.2.6 Nucleic acids alkaline agarose gel electrophoresis 52
7.2.7 Southern blot 53
7.2.8 Dot blot 54
7.2.9 PCR 54
7.2.10 Radioactive labelling by random priming 55
7.2.11 Radioactive end-labelling of telomere probe 57
7.2.12 Detection of hybridization signals 58
7.2.13 TRF (terminal restriction fragments) analysis 58
7.2.14 PETRA (primer extension telomere repeat amplification) 59
7.2.15 PENT (primer extension nick translation) 61
7.2.16 Telomere circle (t-circle) assay 62
7.2.17 Nuclei isolation and chromatin MNase digestion 64
7.2.18 Isolation of telomerase extract 65
7.2.19 Protein concentration assessment 65
7.2.20 TRAP (telomere repeat amplification protocol) 66

8 Results **68**

8.1 Plasmid PCR optimisation 68
8.2 *P. patens* transformation 69
8.3 Analysis of the bulk telomere length in *pptr* mutants 70
8.4 Analysis of telomere lengths on specific chromosome arms 71
8.4.1 PETRA optimisation 71
8.4.2 Telomeres in *pptr* mutants 72
8.5 Analysis of the telomere chromatin structure 74
8.5.1 Optimisation of MNase chromatin digestion 74
8.5.2 Telomere chromatin in *pptr* mutants 76
8.6 Analysis of telomere G-overhangs 77
8.6.1 Optimisation of methods for G-overhangs analysis 77
8.6.2 Telomere G-overhangs in *pptr* mutants 79
8.7 Analysis of ISiT (interstitial sequence within telomeres) 80

8.8 t-circle analysis 81
8.8.1 Optimisation of t-circles analysis 81
8.9 Analysis of telomerase activity 83
8.9.1 Optimisation of TRAP 83
8.9.2 Telomerase activity in *pptr* mutants 85

9 Discussion **86**

10 Conclusion **91**

Bibliography **93**

Appendix A In gel hybridization protocol **104**
A.1 Sample and gel preparation 104
A.2 Native DNA hybridization with a radioactively labelled telomere probe 104
A.3 Denatured DNA rehybridization with a radioactively labelled telomere probe . 105
A.4 Results 105

Appendix B *Arabidopsis thaliana* cultivation **107**

List of Figures

Figure 2.1 The T-loop structure 29
Figure 2.2 G-quartet (left) and intramolecular G-quadruplex (right) structures 30
Figure 2.3 An illustrative scheme of telomeres and its associated proteins in a) human, b) *Arabidopsis thaliana* 32
Figure 3.1 Schematic telomere elongation by telomerase 33
Figure 3.2 Arrangement of TERT functional domains 34
Figure 3.3 Scheme of *P. patens* TR 36
Figure 5.1 Life cycle of *P. patens* 40
Figure 7.1 Scheme of Southern blot apparatus for transfer of DNA fragments from agarose gel to nylon membrane 53
Figure 7.2 Radioactive labelling of the telomere probe by random priming method 56
Figure 7.3 Schematic overview of PETRA workflow 59
Figure 7.4 Scheme of the PENT reaction 61
Figure 7.5 Schematic overview of TRAP 66
Figure 8.1 Plasmid PCR optimisation 69
Figure 8.2 Transformed protoplasts cultivated on BCDAT medium with 6% mannitol 70
Figure 8.3 Bulk telomere lengths analysis using the TRF protocol in stable *pptr* mutant lines and *P. patens* wild-type (wt) 71
Figure 8.4 Optimisation of PETRA 72
Figure 8.5 PETRA analysis of telomere lengths at a) 2R, 3L, b) 10L, 21R, c) 24L, and 24R chromosome arms in stable *pptr* mutants and wild-type moss (wt) 73
Figure 8.6 Selection of extraction buffer for nuclei isolation 74
Figure 8.7 Optimisation of buffer for chromatin MNase digestion 75
Figure 8.8 Optimisation of the amount of MNase for chromatin digestion 76
Figure 8.9 Analysis of the bulk and telomere chromatin structures in *pptr* mutant and wild-type (wt) lines 77
Figure 8.10 Optimisation of annealing and elongation temperatures for the PENT reaction 78
Figure 8.11 Optimisation of the elongation step and DNA polymerase for the PENT 79
Figure 8.12 Telomere G-overhangs analysis in *pptr* mutant and wild-type (wt) lines using the PENT method 80

Figure 8.13 Dotblot analysis of ISiT 81
Figure 8.14 t-circle quantification pilot results in stable pptr mutant line and wild-type (wt) 82
Figure 8.15 C-circles quantification in *pptr* mutant line and wild-type (wt) 83
Figure 8.16 TRAP optimisation of primers combination results 84
Figure 8.17 Analysis of telomerase activity in *pptr* mutants and wild-type (wt) by the TRAP. 85
Figure A.1 In gel hybridization of DNA from *P. patens* wild-type and *A. thaliana* leaves digested by *MseI* with radioactively labelled PlTelC oligonucleotide 106

List of Table

Table 7.1 Plasmids used in diploma thesis 43
Table 7.2 Sequences of primers 47
Table 7.3 Conditions of agarose gel electrophoresis 52
Table 7.4 Conditions of alkaline agarose gel electrophoresis 53
Table 7.5 PCR programs 54
Table 7.6 Non-template PCR program for telomere probe preparation 55
Table 7.7 Reaction mixture for the first step of the PETRA analysis 60
Table 7.8 Conditions of the first step of the PETRA analysis 60
Table 7.9 Reaction mixture for the second PCR step of PETRA analysis 60
Table 7.10 Conditions of the second PCR step of the PETRA analysis 61
Table 7.11 Reaction mixture for t-circle PCR, total volume 20 µl 62
Table 7.12 Reaction mixture for t-circle qPCR, total volume 20 µl 63
Table 7.13 Program for qPCR t-circle analysis 63
Table 7.14 Reaction mixture for the TRAP 66
Table 7.15 Conditions of the TRAP 67

List of Abbreviations

ABA	abscisic acid
ALT	alternative lengthening of telomeres
APBs	ALT-associated PML bodies
ATLAS	advanced telomere length analysis in *S. cerevisiae*
CTE	C-terminal extension
D-loop	displacement loop
DSBs	double-strand breaks
HR	homology recombination
ISiT	interstitial sequence within telomere
MNase	micrococcal nuclease
NLS	nucleus localization-like signal
non-LTR	non-long terminal repeat
PAGE	polyacrylamide gel electrophoresis
PENT	primer extension nick translation
PETRA	primer extension telomere repeat amplification
PML	promyelocytic leukemia
POT1	protection of telomeres 1
pptr	*P. patens* with inactivated TR gene
RAP1	repressor-activator protein 1
STE	stem terminus element
T50	TEX with protein concentration 50 $ng \cdot \mu l^{-1}$
T250	TEX with protein concentration 250 $ng \cdot \mu l^{-1}$
T500	TEX with protein concentration 500 $ng \cdot \mu l^{-1}$
TBE	template boundary element
t-circle	telomere circle
TEN	telomerase essential N-terminal

TERT	telomerase reverse transcriptase
TEX	telomerase extract
TIN2	TRF1-interacting nuclear protein 2
T-loop	telomere loop
TPP1	TIN2- and POT1-organizing protein 1
TR	telomerase RNA
TRAP	telomere repeat amplification protocol
TRBD	telomerase RNA-binding domain
TRF	terminal restriction fragment
TRF1	telomere repeat factor 1
TRF2	telomere repeat factor 2
T-SCE	telomere sister chromatid exchange
TVR	telomere variant repeat

1 Introduction

Telomeres, nucleoprotein structures localized at the ends of linear eukaryotic chromosomes, act as a protection against DNA break repair machinery and gene loss caused by the DNA polymerase inability to replicate chromosome very ends perfectly. In some cells, e. g., human stem cells or plant proliferating meristematic cells, telomeres shortening caused by incomplete DNA replication is compensated by nucleoprotein enzyme, telomerase.

In specific cases, telomere maintenance can be secured by telomerase-independent mechanisms, alternative lengthening of telomeres (ALT). The ALT is typical in tumours; 10–15% of cancer cells are able to elongate telomeres without active telomerase. Furthermore, ALT was identified in mutant plants, e. g. in *A. thaliana* TERT mutants or *P. patens* TR mutants.

2 Telomeres

Linear structure of eukaryotic chromosomes poses two main problems for organisms: (a) the necessity of distinguishing the chromosome ends from the double strand breaks (DSBs; end-protection problem), and (b) to compensate the incomplete replication of chromosome ends leading to theirs progressive shortening during cell divisions (end-replication problem). The end-protection problem arises from possible recognition of natural chromosome ends by DNA repair machinery which could lead to possible end-to-end chromosome fusion and thus interruption of genome stability (McClintock, 1942, 1938; Müller, 1938). On the other hand, the progressive shortening of chromosomes is a potential risk of gene loss (Olovnikov, 1971). Solution for both problems is the presence of nucleoprotein structures, termed telomeres, localized at the ends of linear eukaryotic chromosomes and their associated proteins.

2.1 Structure of telomeres

Telomeres are repetitive non-coding tandem repeats with variable sequence. Among vertebrates, the human-type $(TTAGGG)_n$ sequence is very conserved (Burki et al., 2020). For insect, the $(TTAGG)_n$ sequence is typical (Vítková et al., 2005). At the same time, telomeres of some insect species are composed of unusual telomere motifs derived from non-LTR (non-long terminal repeats) retrotransposons. The non-LTR retrotransposon telomeres are typical for insects with weak expression of the *TERT* gene, like *Bombyx mori*, or for *Drosophila melanogaster*, in whose the *TERT* gene is completely missing (Casacuberta, 2017; Fujiwara et al., 2005; Sasaki and Fujiwara, 2000; Takahashi et al., 1997). Telomere sequence TG_{1-3} was found in *Saccharomyces cerevisiae* (Wellinger and Zakian, 2012).

In Arachaeplastida supergroup (including red and green algae, mosses, and land plants), canonical $(TTTAGGG)_n$ telomere sequence was first described in the model plant *Arabidopsis thaliana* (Richards and Ausubel, 1988). However, many different telomere repeats were characterized in representatives of this group, e.g., human-type sequence in some species of the order Asparagales (Sýkorová et al., 2006), completely unusual $(CTCGGTTATGGG)_n$ sequence in the Allium species (Fajkus et al., 2016), $(TTTTTTAGGG)_n$ in *Cestrum* (Solanaceae) (Peška et al., 2015), or $(TTCAGG)_n$ and $(TTTCAGG)_n$ in carnivorous plants *Genlisea hispidula* and *G. subglabra* (Tran et al., 2015).

Telomeres are very variable in their lengths, which differ not only across different species but also among individuals of one species. It was also reported that even different chromosome arms within a single cell can have variable telomere lengths (Heacock et al., 2004).

The double-stranded telomeres are terminated by a single-stranded 3' overhang located at the G-rich strand, termed G-overhang. The overhang can fold back with help of telomere associated proteins, invades into double-stranded part of the telomere and hides its end into so-called D-loop (displacement loop). This process leads to creation of a tertiary telomere lasso-like structure known as a telomere loop (T-loop, **Figure 2.1**). The T-loop is one of the mechanisms of chromosome ends protection as it prevents the telomere end to be recognized by DNA repair machinery (Griffith et al., 1999; Lange, 2005).

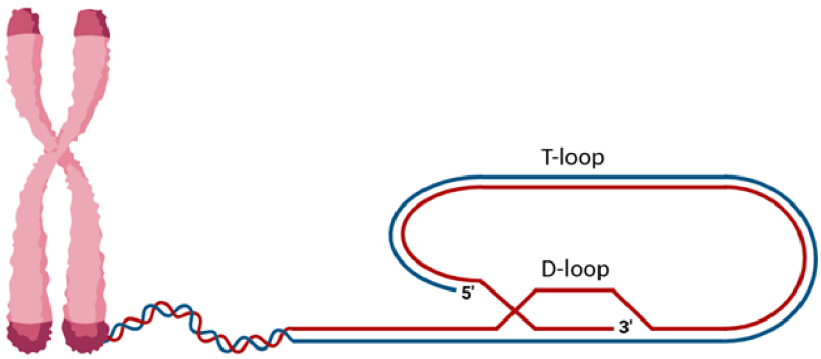

Figure 2.1 The T-loop structure. 3' G-overhang invades the double-stranded part of the telomere and create the D-loop.

As the telomeres are rich in guanines, they can form another higher order structure – the G-quadruplexes (Rhodes and Lipps, 2015). G-quadruplexes create a structural barrier for binding of DNA repair proteins and so contribute to the protection of chromosome ends (Wang et al., 2011). The G-quadruplexes can be formed between two or more G-quartets stacked on top of each other. The G-quartets are created thanks to non-canonical Hoogsteen base-pairing between four guanines (**Figure 2.2**) (Rhodes and Lipps, 2015; Sen and Gilbert, 1988).

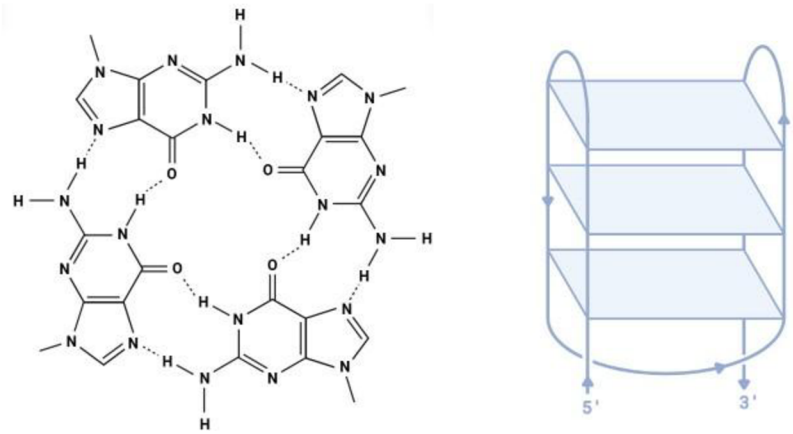

Figure 2.2 G-quartet (left) and intramolecular G-quadruplex (right) structures. Four guanines are stabilized by Hoogsteen base-pairing forming G-quartet. Multiple G-quartets can be stacked on top of each other and form G-quadruplex.

2.2 Telomere-associated proteins

Telomeres alone are unable to fulfil their function. The solution of the end-replication problem, specifically the elongation/maintenance of telomeres, is accomplished by the telomerase enzyme (see **section 3**). On the other hand, distinguishing the chromosome ends from DNA damage sites requires cooperation of other proteins associated with telomeres.

In humans, the telomere-associated protein complex is called shelterin (**Figure 2.3 a**). It includes dsDNA binding proteins TRF1 (telomere repeat-binding protein 1), TRF2 (telomere repeat-binding protein 2), ssDNA binding protein POT1 (protection of telomeres 1), and proteins bind via protein-protein interactions: TIN2 (TRF1-interacting nuclear protein 2), TPP1 (TIN2- and POT1-organizing protein 1), RAP1 (repressor-activator protein 1). Shelterin-like protein complexes are present among all vertebrates (Lange, 2005).

The specificity of shelterin complex to telomere DNA is ensured by C-terminal myb domains of TRF1 and TRF2 proteins which recognized `YTAGGGTTR` sequence. To increase the binding specificity, both proteins form a homodimer and higher-order oligomers via TRFH domains (Broccoli et al., 1997). Next, POT1 binds `(T)TAGGGTTAG` sequence with two N-terminal OB folds and creates a heterodimer with TPP1 (Lei et al., 2004).

The TIN2 protein function as a backbone ensuring the connection of TRF1, TRF2, and TPP1 proteins through protein-protein interactions (Lange, 2005). Interestingly, shelterin can be partitioned into two subcomplexes differing in their binding principle. While TRF1-TIN2-

TPP1-POT1 subcomplex binds strongly to telomere DNA, the TRF2-RAP1 dimer is associated more dynamically (Janovič et al., 2025).

The shelterin participate in inhibition of DNA damage response (Sfeir and de Lange, 2012; Zimmermann et al., 2013), telomerase recruitment (Latrick and Cech, 2010; Schmidt and Cech, 2015), formation of T-loops (Stansel et al., 2001), and facilitation of replication fork movement through telomeres (Sfeir et al., 2009).

The TPP1 protein together with POT1 recruit the telomerase to the telomere and limits its activity to prevent telomere overextension. Furthermore, the POT1 protein hides G-overhang from DNA damage response and regulates the accessibility of telomerase to telomeres (Zhong et al., 2012). The TRF1 promoted the telomere replication (Zimmermann et al., 2014), and TRF2 is responsible for T-loops formation and non-homologous end joining repression (Timashev and De Lange, 2020). Furthermore, it can create a heterodimer with RAP1, which regulates the binding to telomere DNA and thus enables the processing of telomere loop with helicases (Janoušková et al., 2015).

On the other hand, in plants, only telomere repeat binding (TRB) proteins, members of a single-myb-histone family, were identified in *Arabidopsis thaliana* and their orthologues in other plants, as proteins binding to telomeres (**Figure 2.3 b**) (Kuchař and Fajkus, 2004; Kusová et al., 2025; Marian et al., 2003; Procházková Schrumpfová et al., 2014). TRB proteins bind DNA via telobox, a myb-like DNA-binding motif located at the N-terminus (Bilaud et al., 1996; Peška et al., 2011). TRF-like proteins were also identified in plants. However, it seems that they did not play a role in telomere maintenance (Fulcher and Riha, 2016).

The TRB proteins possess central histone-like (H1/5) domain facilitating DNA sequence-nonspecific protein interactions with DNA, their dimerization, and interaction with POT1b. In *A. thaliana*, TRB protein family consists of five proteins interacting with each other, and with telomerase TERT subunit (Kusová et al., 2023; Simonet et al., 2011). TRB proteins are crucial for telomere maintenance not only in flowering plants, but also in mosses, such as *Physcomitrium patens*, in which three TRB proteins are working in harmony to ensure telomere stability and cell viability (Kusová et al., 2025).

Besides TRBs, three paralogous of POT1 protein were identified in *A. thaliana* – POT1a, POT1b, and POT1c. The POT1a protein not only binds to telomeres but also interacts with telomerase and positively regulates its activity. POT1b ensures the chromosome end protection and interacts with telomere indirectly through TRB1 protein. Last, POT1c protein, has very low

expression due to the transposon invasion of the promotor which led to permanent gene silencing. This happened early after its formation by POT1a locus duplication (Kobayashi et al., 2019; Procházková Schrumpfová et al., 2014).

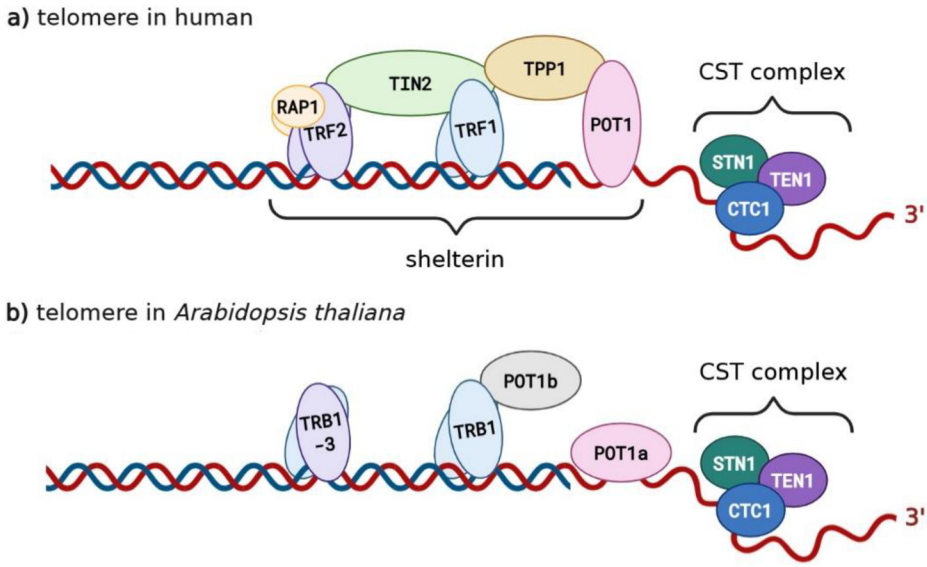

Figure 2.3 An illustrative scheme of telomeres and its associated proteins in **a)** human, **b)** *Arabidopsis thaliana*. Created according to Procházková Schrumpfová et al. (2019).

Besides shelterin in mammals and its equivalents in plants, another complex associated with telomere maintenance mechanism was identified in plants, mammals and yeasts. The CST complex is a heterotrimer composed of three proteins – CTC1, STN1, and TEN1. In yeasts Cdc13 protein occurs in CST complex instead of CTC1. It accesses the telomeres through single-strand 3' G-overhang and helps to balance the telomere maintenance mechanism (reviewed in Lim and Cech, 2021). The CTC1 and STN1 proteins prevent the over-extension of G-overhangs, while TEN1 protein plays crucial role in C-strand fill-in synthesis by recruiting the DNA polymerase α (Feng et al., 2018).

3 Telomerase

The end-replication problem is resolved by the ribonucleoprotein complex – telomerase. It has the ability to elongate telomeres by its reverse transcriptase activity. The catalytic function is provided by the telomerase reverse transcriptase (TERT) protein subunit, and the template for reverse transcription is served by the telomerase RNA (TR). TR subunit also navigates the telomerase complex to the chromosome ends (**Figure 3.1**). The core telomerase complex subunits are associated with other proteins, which facilitates telomerase assembly, localization, trafficking, recruitment to telomeres, or telomere synthesis processivity.

Figure 3.1 Schematic telomere elongation by telomerase. Telomerase RNA (TR) subunit binds to telomere G-overhang and serves as a template for the telomerase reverse transcriptase (TERT) protein subunit with catalytic activity.

In humans, telomerase is active in all early developmental stages, with progressively increasing activity in advanced embryo stages. After the organogenesis is finished, telomerase activity is restricted to stem cells (reviewed in Procházková Schrumpfová et al., 2019). The downregulation of telomerase activity in somatic cells reduce the risk of cancer. The reactivation of telomerase is connected with cell immortality and tumorigenesis (Shay and Wright, 2005).

Telomerase activity is also strictly regulated in plants. Similarly, as in human cells, its activity is downregulated in terminally differentiated tissues (e.g., stems or mature leaves). Active telomerase is detected in highly proliferating meristematic cells – e.g., seedlings, root tips, young leaves, flowers, or floral buds. The re-activation of telomerase can occur in secondary

meristem which arises from differentiated cells or during plant regeneration (Fajkus et al., 1998, 1996; Fitzgerald et al., 1996; Riha et al., 1998).

The telomerase, catalysed nucleotide addition to the 3' hydroxyl group. The TR navigates whole complex to the very end of G-overhang and let the telomerase binds on it through its few first oligonucleotides. After G-overhang extension, its interaction with template is dissociated. However, telomerase complex is not fully dissociated from telomere end so it could process another round of the G-overhang extension. The complementary telomere C-strand is synthesized by fill-in synthesis with DNA polymerase α which is recruited to telomeres by a CST complex (Wu et al., 2017).

3.1 Telomerase reverse transcriptase (TERT)

The TERT subunit cares the catalytic activity of telomerase. TERT protein is highly conserved, despite the gene structure, which differ among groups of organisms (reviewed in Schrumpfová and Fajkus, 2020). The protein structure can be divided into three major parts: N-terminal part, central reverse transcriptase (RT) domain, and C-terminal extension (CTE) (**Figure 3.2**).

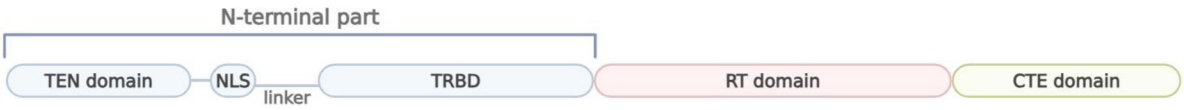

Figure 3.2 Arrangement of TERT functional domains. N-terminal part with two main domains: TEN (telomerase essential N-terminal) domain, and TRBD (telomerase RNA-binding domain) separated with linker containing NLS (nucleus localization signal). The central RT (reverse transcriptase) domain with evolutionary-conserved RT motifs. The CTE (C-terminal extension) domain.

The N-terminal part contains two main domains – telomerase essential N-terminal domain (TEN), and the telomerase RNA-binding domain (TRBD) – separated with linker. Nucleus localization signal (NLS), which is responsible for transport of the TERT protein subunit into the nucleus, is recognized between these two domains (Chung et al., 2012; reviewed in Sýkorová and Fajkus, 2009). The RT domain bears the catalytic activity and contains evolutionary conserved RT motifs. There are two subdomains recognized within the RT domain. The "fingers" ensures the nucleotide binding and enzyme processivity, and the "palm" provides DNA primer grip and polymerase catalytic residues (Lingner et al., 1997; Nakamura et al., 1997). The CTE domain is strongly conserved, although it is not involved in essentials telomerase

functions. It is suggested that the CTE domain participates in promoting the telomerase processivity, regulation of telomerase localization, and in differential binding of DNA (reviewed in Autexier and Lue, 2006).

Although the TERT protein is conserved, the gene structure differs among groups of organisms with respect to the exon/intron organisation (reviewed in Schrumpfová and Fajkus, 2020).

3.2 Telomerase RNA (TR)

The TR subunit of telomerase is a non-coding RNA, in plants and ciliates product of RNA polymerase III (Fajkus et al., 2019), in mammals and yeasts of RNA polymerase II (Podlevsky and Chen, 2016). TR contains a region that serves as a template for addition of telomere repeats through the reverse transcription process. Its sequence reflects the telomere repeat of the respective organisms. The TR is highly divergent – mainly in size and sequence – compared to the TERT protein subunit. The TR size ranges from lower hundreds to higher thousands nucleotides. Despite its sequence variability, conserved structural domains/secondary structures were found in TR – such as pseudoknot, template boundary element (TBE), or stem-loop region (STE). All of these elements are crucial for biogenesis, stability, and regulation of telomerase complex (Egan and Collins, 2012; Fajkus et al., 2021; Webb and Zakian, 2016).

P. patens TR (**Figure 3.3**) belongs with its 238 nucleotides to relatively short TRs. The template sequence is bordered with TBE (P1.1) at 5' end of template, and template recognition element (P2.1) at 3' end; both are plant-specific stem loops. The template region possesses UCAACCCUAAACC sequence (Box et al., 2008; Bozděchová et al., 2024). This sequence, especially the CCC triplet, was thought to be highly reactive to chemical probing because it should act as a template for telomere synthesis. However, Bozděchová et al. (2024) discovered that the triplet in, DMS *in vivo* and SHAPE *in vitro* treatments remained intact. This discovery led to hypothesizing about two statuses of *P. patens* TR – OPEN and CLOSED. Detailed analysis showed that *in vivo*, one of four possible structures of TR is OPEN and therefore sensitive to DMS treatment. Same phenomenon of two TR statuses was uncovered in corresponding CCC triplet in *Tetrahymena* (Cole et al., 2012), human, and *A. thaliana* TRs (Antal et al., 2002; Song et al., 2019). Therefore, the triplet seems to be a conserved motif creating the border between

the end of the active site where telomere lengthening takes place, and telomere repeat in the template region (Choi et al., 2022; Niederer and Zappulla, 2015; Peska and Garcia, 2020).

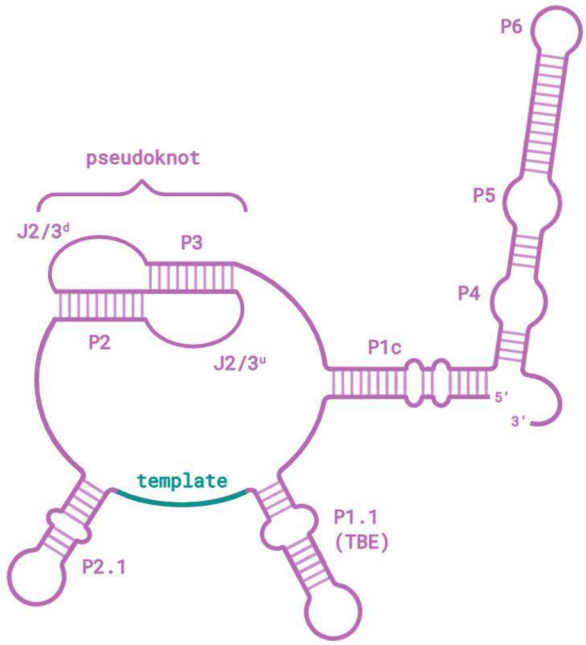

Figure 3.3 Scheme of *P. patens* TR. P1.1, which corresponds to TBE conserved domain, and P2.1, which is thought to act as template recognition element, are plant-specific stem loops. Template region is located between these two plant-specific stem loops (in green). The position of conserved CCC motif within the template is connected with OPEN and CLOSED statuses of TR. Another highly conserved domain, the pseudoknot, comprised P2 (G-C rich) and P3 which are connected with J2/3^{u} with invariant U residues and J2/3^{d} loops. The pseudoknot in *P. patens* is present only in OPEN active status of TR. The flexible core region is closed by P1c helix. Less reactive rigid region contains short stems with inserted bulges (P4, P5, and P6). The illustration was created according to Bozděchová et al. (2024); Fajkus et al. (2021).

4 Alternative Lengthening of Telomeres (ALT)

In most cells, telomeres are elongated through telomerase. Besides telomerase, the telomere length can be maintained through telomerase-independence mechanism, so-called ALT. It is a homology-directed repair-like mechanism which can be activated as a back-up in telomerase-deficient organisms.

The ALT occurs in 10–15% of cancer cells, which can lead to the resistance to treatment with telomerase inhibitors (Hu et al., 2012). The utilization of telomerase-independent mechanism for the telomere maintenance was also described in plants. It was activated in *A. thaliana* mutants lacking the TERT subunit (Růčková et al., 2008), or *P. patens* TR subunit knock-out mutants (Fajkus et al., 2021).

The telomeres elongated by became heterogenous in their length (Bryan et al., 1995) and sequence (Conomos et al., 2013; Lee et al., 2014). Despite changes in telomeres themselves, ALT cells possess elevated frequency of telomere sister chromatid exchanges (T-SCEs; Londoño-Vallejo et al., 2004).

One of the most significant features of ALT cells is the presence of an extrachromosomal telomere DNA in many different forms, e.g., double- or single-stranded circles or linear double-stranded telomere DNA. The double-stranded telomere circles (t-circles) can result from D-loop formation by recombination enzymes as the prevention of telomere overextension (Cesare and Reddel, 2010). More specific for ALT are single- or partially double-stranded C-circles. It can be speculated, that C-rich (or G-rich, however these are less abundant) can arise form t-circles by nucleolytic degradation of one strand (Henson et al., 2009).

In human cells, telomere DNA, homology recombination (HR) factors, and shelterin complex are all grouped in specific subclass of promyelocytic leukemia (PML) nuclear bodies. The presence of PML bodies is characteristic for ALT cells, and these are therefore termed ALT-associated PML bodies (APBs; reviewed in Cesare and Reddel (2010).

Furthermore, ALT cells have increased content of telomere variant repeats (TVRs). TVRs are common in proximal telomere region, however in ALT cells, they are present also in distal regions (Lee et al., 2014). In human ALT cells, `TGAGGG`, `TTGGGG`, and the most typically `TCAGGG` TVRs are enriched in telomeres (reviewed in Conomos et al., 2013). All types of TVRs caused disruption of binding of telomere binding proteins. Lower content of shelterin together with newly created binding sites create a space for altered telomere binding proteins. E. g., the

TCAGGG TVR is sequence-specifically bound by proteins from nuclear receptors group, e. g., COUP-TF1, COUP-TF2, TR2, TR4, and EAR2 (Conomos et al., 2012; Déjardin and Kingston, 2009; Marzec et al., 2015).

5 Physcomitrium patens

Physcomitrium patens is a monocotyledonous plant from *Funariaceae* family within *Funariales*. Based on fylogenetic and fylogenomic, genus *Physcomitrella* was renamed to *Physcomitrium* (Beike et al., 2014; Medina et al., 2019, 2018).

The genome of *P. patens* was the first sequenced genome among bryophytes and the fourth among plant model species (Rensing et al., 2008). The *P. patens* genome comprises of 500 Mbp organized into 27 chromosomes. Genes and transposable elements are evenly distributed along chromosomes (Lang et al., 2018).

Physcomitrium patens is widely used for study of biological processes, mainly in cellular and evolutionary contexts. In these days, it is often used in functional genomics for study of protein functions, since the *P. patens* allows effective genes integration through HR-mediated gene targeting and therefore an easy genome editing (Cove, 2005; Cove et al., 2009; Kamisugi et al., 2006; Schaefer, 2002; Schaefer and Zrÿd, 1997). Huge advantage of *P. patens* as model organism is its easy cultivation and fast development of filamentous protonemas. Protonema cells are accumulated in G2/M phase, which is connected with higher frequency of HR. *P. patens* is therefore an ideal candidate for functional studies (Cove et al., 2009; Schween et al., 2003).

The elevate frequency of HR reflects preferred DSBs repair mechanism. The *P. patens* primary and sufficiently repairs DNA breaks by HR. The mutation of both RAD51 proteins, essential factors of HR, results in markedly increased sensitivity to DNA damage factors. Despite HR, non-homology end joining repair mechanism is also present in *P. patens.* However, it does not play an important role in DSBs repair it is important as a backup in case of HR absence (Angelis et al., 2023; Fojtová et al., 2015b; Goffová et al., 2019)

5.1.1 Life cycle

The *P. patens* life cycle can be dived into dominant haploid gametophytic phase and diploid sporophytic phase, both multicellular (**Figure 5.1**).

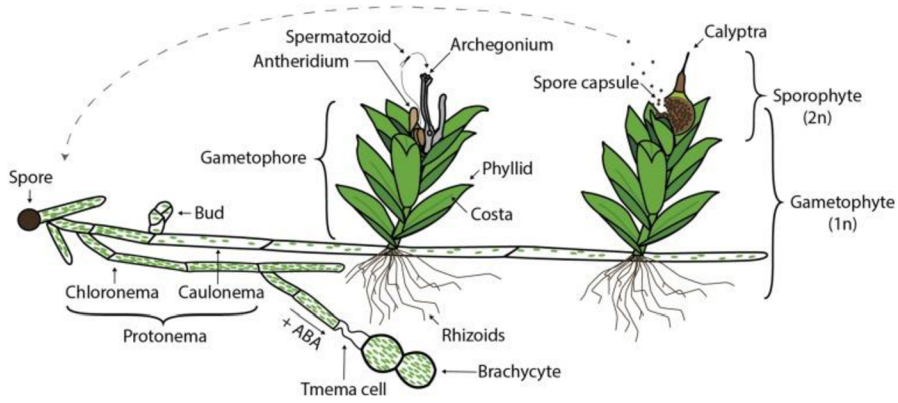

Figure 5.1 Life cycle of *P. patens* (Rensing et al., 2020).

Starting from the spore germination, it develops into branched protonema, juvenile gametophyte phase, comprising two types of cells – chloronema and caulonema. Chloronema the most basal cell, the first growing from the spore, is rich in huge chloroplasts and provides photosynthesis. Chloronema can give arise to caulonema or brachycyte (Menand et al., 2007; Rensing et al., 2020).

Brachycyte is a vegetative diaspore which evolved from chloronema cells in the presence of abscisic acid (ABA). It is a terminal ontogenetic stadium for the ABA pathway (Arif et al., 2019). On the other hand, under auxin and cytokinin treatment, caulonema is developed. It disposes with less amount of small less developed chloroplasts and served as a nutrition collector (Coudert et al., 2015; Menand et al., 2007).

From caulonema, brunch initials (so-called buds) representing the start of the three-dimensional growth phase are developed. They give arise to gametophores which are structured into stem and phyllids. On adult gametophores, gametangiogenesis occurs. One plant possesses both male and female gametangias (Coudert et al., 2015; Cove and Knight, 1993; Rensing et al., 2020).

First, antheridia develop at the apex of the stem in which male gametes spermatozoids (also known as sperm cells or antherozoids) are created. Later, the stem continues to growth to developed archegonia with female gametes termed oogonia (or egg cells). Mature spermatozoids are biflagellate and therefore need water film to successfully swim to archegonium and fertilize the egg cell. Diploid zygote developed into an embryo and then into a sporophyte with a single spherical capsule on a short stalk. The capsule is covered by a thin hood termed

calyptra and can contain up to 5,000 haploidic spores which are released irregularly from the lower parts of mature capsule (Cove and Knight, 1993; Hiss et al., 2017; Rensing et al., 2020).

6 Aims of Thesis

The first aim of the diploma thesis was to analyse *Physcomitrium patens* mutants with loss of function of the gene encoding telomerase RNA (*pptr*) with respect to the length and structure of telomeres.

Second aim was to prepare new *pptr* mutants for further studies of the dynamics of changes of telomere length and structure during the switch from telomerase-dependent to telomerase-independent mechanism of the telomere maintenance.

7 Material and Methods

7.1 Material

7.1.1 Plant material

Physcomitrium patens protonema was used for all experiments. *P. patens* stable mutant line (*pptr*) was described previously in Fajkus et al. (2021).

7.1.2 Plasmids

Plasmids *Cas9* and *TR_KO* (**Table 7.1**) for construction of new *pptr* mutants were kindly provided by Marcela Holá from Institute of Experimental Botany, CAS, Prague. *TR_KO* plasmid carries a gene for hygromycin resistance with boundary sequences homologous to DNA segments delimiting TR in the *P. patens* genome. The TR gene is replaced by the gene for hygromycin resistance based on this homology.

Table 7.1 Plasmids used in diploma thesis.

Label	Construct	Bacteria ATB resistance	*P. patens* ATB resistance
Cas9	pMKCas9_sgRNA	ampicillin	kanamycin
TR_KO	TR_KO_35S_Hygro	kanamycin	hygromycin

7.1.3 Chemicals and solutions

- α-^{32}P-dATP — IZOTOP
- γ-^{32}P-ATP — IZOTOP
- φ29 reaction buffer — 10× concentrated; New England Biolabs
- AA:BIS (19:1) — 40%; SERVA
- Agarose — SERVA
- Alkaline electrophoresis running buffer — 30 mM NaOH; 2 mM EDTA, pH 7.5
- Alkaline electrophoresis gel buffer — 30 mM NaCl; 2 mM EDTA, pH 7.5

• Alkaline electrophoresis loading buffer	6× concentrated; 180 mM NaOH, 6 mM EDTA, 18% Ficoll 400, 0.15% bromophenol blue, 0.25% xylene cyanol
• Ammonium acetate	2 M; pH 7.0
• Ammonium persulfate	30%; SIGMA
• Ammonium tartrate	250 mM
• Ampicillin	Duchefa Biochemie
• B solution	101 mM $MgSO_4 \cdot 7H_2O$
• Bradford dye reagent	SIGMA
• BSA	10 $mg \cdot ml^{-1}$; New England Biolabs
• BTE buffer	50 mM Tris-HCl, pH 8.0; 1 mM EDTA, pH 8.0
• C solution	367 mM KH_2PO_4
• Calcium chloride	1 M
• Chloroform	PENTA
• D solution	1 M KNO_3; 5 mM $FeSO_4 \cdot 7H_2O$
• Denhardt's hybridization solution	5× SSC; 5× Denhardt's reagent; 50 mM NaH_2PO_4; 1 $g \cdot l^{-1}$ BSA
• Denhardt's reagent	100× concentrated; 2% Ficoll 400, 2% polyvinylpyrrolidone, 2% BSA
• DMSO	SIGMA
• DNA denaturation solution	0.4 M NaOH; 10 mM EDTA
• DNA ladder	GeneRuler 1 kb DNA; Thermo Fisher Scientific
• DNA loading buffer	6× concentrated; 0.25% bromophenol blue, 0.25% xylene cyanol, 40% sucrose
• dNTPs	25 mM each (dATP, dCTP, dGTP, dTTP); TaKaRa
• DreamTaq reaction buffer	10× concentrated; Thermo Fisher Scientific
• Driselase	2%; SIGMA
• DTT	1 mM
• EB buffer	100 mM Tris-HCl, pH 8.0; 50 mM EDTA, pH 8.0; 500 mM NaCl; 10 μM β-mercaptoethanol

• Elizyme™ Green Mix Ad-dROX	2× concentrated; Elisabeth Pharmacon
• Ethanol	96%; Lachner
• Ethidium bromide	1 mg·ml^{-1}; SERVA
• ExTaq reaction buffer	10× concentrated; TaKaRa
• Glycerol	PENTA
• GelStar	Lonza
• GlycoBlue™ Coprecipitant	15 mg·ml^{-1}; Thermo Fisher Scientific
• Hybridization solution	0.25 M sodium phosphate; 7% SDS; 16 mM EDTA, pH 7.5
• Hydrochloric acid	35%; PENTA
• Isoamylalcohol	PENTA
• Isopropanol	PENTA
• Kanamycin	Duchefa Biochemie
• LB medium	Luria-Bertani medium; 10% tryptone, 20% yeast extract, 171 mM NaCl; pH 7.0
• Mannitol	PENTA
• MMg solution	0.4 M mannitol; 15 mM $MgCl_2$; 4 mM MES, pH 5.7
• MyTaq reaction buffer	5× concentrated; Bioline
• Nuclei isolation buffer	15 mM PIPES, pH 6.8; 5 mM $MgCl_2$; 60 mM KCl; 15 mM NaCl; 1 mM $CaCl_2$; 0.9% Triton X-100; 0.5 M saccharose
• Nucleosome buffer	50 mM Tris-HCl; 125 mM sucrose; 5 mM $MgCl_2$; 3 mM $CaCl_2$; 10 mM β-mercaptoethanol; 250 µM spermidine; 100 µM PMSF
• PEG/Ca solution	0.6 g·ml^{-1} PEG 4000; 0.3 M mannitol; 150 µM $CaCl_2$
• PEG 8000	SIGMA
• Phenol	PanReac AppliChem
• Potassium acetate	5 M; pH 7.0
• Q5 reaction buffer	5× concentrated; New England Biolabs
• rCutSmart buffer	10× concentrated; New England Biolabs
• SDS	20%; SIGMA

- S.O.C. medium — 2% tryptone; 0.5% yeast extract; 10 mM NaCl; 2.5 mM KCl; 10 mM $MgCl_2$; 10 mM $MgSO_4$; 20 mM glucose
- Sodium acetate — 3 M; pH 7.0
- Sodium hydroxide — 0.4 M; PENTA
- SSC — 20× concentrated; 0.3 M sodium acetate, 3 M NaCl
- StandardTaq reaction buffer — 10× concentrated; New England Biolabs
- STOP buffer — 1% sarcosyl; 0.5 M EDTA; 2 M NaCl
- T4-PNK buffer — 10× concentrated; New England Biolabs
- TAE buffer — 1 mM EDTA, 50 mM Tris-acetate; pH 8.0
- TBE buffer — 450 mM Tris-borate; 10 mM EDTA, pH 8.3
- t-circle buffer — 0.2 M Tris-HCl, pH 7.5; 0.2 M KCl; 1 mM EDTA
- TE buffer — 10 mM Tris-HCl, pH 8.0; 1 mM EDTA, pH 8.0
- TEMED — SIGMA
- Trace elements solution — 220 µM $CuSO_4 \cdot 5H_2O$; 10 mM H_3BO_3; 231 µM $CoCl_2 \cdot 6H_2O$; 103 µM $Na_2MoO_4 \cdot 2H_2O$; 191 µM $ZnSO_4 \cdot 7H_2O$; 2 mM $MnCl_2 \cdot 4H_2O$; 169 µM KI
- Tris-HCl — 10 mM
- Tween — 20%; SIGMA
- W buffer — 50 mM Tris-acetate, pH 7.5; 5 mM $MgCl_2$; 100 mM potassium glutamate; 20 mM EGTA, pH 8.0; 1.5% PVP; 10% glycerol; 2 mM DTT; 0.2 mM PMSF; 1.2 mM vanadylribonucleoside complex; 2 $\mu g \cdot ml^{-1}$ pepstatin A; 4 $\mu g \cdot ml^{-1}$ leupeptin
- W5 solution — 154 mM NaCl; 125 mM $CaCl_2$; 5 mM KCl; 2 mM MES, pH 5.7
- Washing solution I — 2× SSC; 0.1% SDS
- Washing solution II — 0.2× SSC; 0.1% SDS

7.1.4 Primers

Primers for PCR amplification of the probe for quantification of interstitial sequences into telomeres (ISiT left and right) were designed with the Primer3 online tool. TR_KO downstream

and upstream primers were kindly provided by Marcela Holá. All other primers were available in the Fajkus's lab.

Table 7.2 Sequences of primers.

Name	Sequence (5' → 3')
47F	CGCGGTAGTGATGTGGTTGTGTT
CAMV	CGTCTTCAAAGCAAGTGGATT
ISiT (forward)	AGCAATAGGATGGAGTGGCA
ISiT (reverse)	TGGTGTCTAGGATGTCAATGGT
PETRA-A	CTCTAGACTGTGAGACTTGGACTAC
PETRA-T	CTCTAGACTGTGAGACTTGGACTACCCTAAACCCT
PlTelC	TGTTAGGTATCCCTAAACCCTAAACCCTAAACCCTAAACCCTAAAACA
PlTelG	ACACTAAGGTTTAGGGTTTAGGGTTTAGGGTTTAGGGTTAGTGT
Pp2R	AATGCGTACTGAACACTGCT
Pp3L	GGCAGGTTCAAAACAGTGAGC
Pp9L	GAAGGTATGTCATGGCCTCAAAGCT
Pp10L	CTCCTCTGGTACACTCAATCC
Pp21L	TACCTATAATACTGGGAGCATCG
Pp21R	CTCATGTCTCTGAAGTTGTGGT
Pp24L	CTCAACCTACATTCTTCTTCCAC
Pp24R	CATTAGGTCAATGTAGAGGTTGC
PpTelPr	GCCTTAACCCTAAACCCTAAAC
PpTS	TCACATTGTTCTCACTCAGGT
PpTS2	CTCATTGTTCTCACTCAGGTT
TelA	CCCCGGTTTTGGGTTTTGGGTTTTGGGTTTTGGGT
TelB	GGGGCCCTAATCCCTAATCCCTAATCCCTAATCCCT
TelPr	CCGAATTCAACCCTAAACCCTAAACCCTAAACCC
ThioTel	$(CCCTAAA)_3$ with thiophosphate linkages between three 3' terminal nucleotides
TR_KO (forward)	GCGCCGTCTCGCTCGGGAGCGTGCTCAAGTATTTTTCTGTTC
TR_KO (reverse)	GCGCCGTCTCGCTCAAGCGCCTCGATCGAATTCGCGATG
TS21	GACAATCCGTCGAGCAGAGTT

Name	Sequence (5' → 3')
Ubiquitin (forward)	ACTACCCTGAAGTTGTATAGTTCGG
Ubiquitin (reverse)	CAAGTCACATTACTTCGCTGTCTA

7.1.5 Enzymes

- φ29-DNA polymerase — 10 000 U·ml^{-1}; New England Biolabs
- DreamTaq DNA polymerase — 5 000 U·ml^{-1}; Thermo Fisher Scientific
- ExTaq DNA polymerase — 5 000 U·ml^{-1}; TaKaRa
- HinfI — 10 000 U·ml^{-1}; New England Biolabs
- HotStartTaq DNA polymerase — 5 000 U·ml^{-1}; New England Biolabs
- Micrococcal nuclease (MNase) — 30 000 U·ml^{-1}; New England Biolabs
- MseI — 10 000 U·ml^{-1}; New England Biolabs
- MyTaq DNA polymerase — 5 000 U·ml^{-1}; Bioline
- NotI-HF — 20 000 U·ml^{-1}; New England Biolaps
- Proteinase K — 20 mg·ml^{-1}; SIGMA
- RNase A — 10 mg·ml^{-1}; SIGMA
- RsaI — 10 000 U·ml^{-1}; New England Biolabs
- SspI — 5 000 U·ml^{-1}; New England Biolabs
- T4 polynucleotide kinase (T4-PNK) — 10 000 U·ml^{-1}; New England Biolaps
- Q5 HotStart High-fidelity DNA polymerase — 2 000 U·ml^{-1}; New England Biolaps

7.1.6 Commercial kits

- DecaLabel DNA Labelling Kit — Thermo Fisher Scientific
- Gen Elute™ Plasmids Miniprep Kit — Sigma-Aldrich
- Genomic DNA ScreenTape Assay — Agilent
- OneShot™ TOP 10 Chemically Competent *E. coli* — Thermo Fisher Scientific
- Qubit™ 1 dsDNA BR Working Solution — Thermo Fisher Scientific

7.1.7 Instruments

• Centrifuges	5804 R	Eppendorf
	3K30	SIGMA
• Dot Blot apparatus	Bio-Dot™	Bio-Rad
• Electrophoretic tanks	Sub Cell GT	Bio-Rad
	SE 600	Hoefer
• Fluorometer	Qubit™ 4	Invitrogen
• Gel Dryer	EC355	E-C Apparatus Corporation
• Gel imaging device	FUSION FX	Vilber Lourmat
• Homogenizer	Silamat S6	Ivoclar Vivadent
• Hybridization oven	ProBlot™	Labnet
• Lyophilizer	ALPHA 2-4 LSCplus	CHRIST
• PCR cycler	ProFlex	Applied Biosystems
• Phosphoimager	Typhoon FLA 9 500	GE Healthcare Life Sciences
• qPCR cycler	Rotor-Gene 6000	QIAGEN
• Refrigerated Vapor Trap	RVT100	Savant
• Shaker	KS 130 Orbital Shaker	BioSan
• Shaking incubator	NB-205VQ	N-BIOTEK
• Spectrophotometer	NanoDrop 2000c UV-Vis	Thermo Fisher Scientific
	DU 730	Beckman Coulter
• Sterile box	Biohazard flow box	TRIGON PLUS
• TapeStation	2200 TapeStation system	Agilent
• Thermoblock	Thermomixer comfort	Eppendorf
• Vacuum pump	VLP120	Savant
• Vortex	Lab dancer	IKA

7.2 Methods

7.2.1 Cultivation of *Physcomitrium patens*

For 1 l of BCDAT medium for *P. patens* cultivation, 10 ml of B solution, 10 ml of C solution, 10 ml of D solution, 10 ml of ammonium tartrate solution, and 1 ml of trace elements solution

were mixed with 8 g of plant agar and distilled water, and the pH was adjusted with KOH to 5.9. The cultivation medium was sterilised in a pressure cooker and cooled. 1 M $CaCl_2$ was added to a final concentration of 1 mM and the BCDAT medium was poured into a Petri dish. A cellophane circle filter (325 P Cellulose; diameter 80 mm) was placed onto a solidified medium.

P. patens culture was homogenized in distilled water and poured onto a cellophane filter in the Petri dish. The moss protonemata were cultivated in a phytotron under long-day conditions: 16 h of light (illumination 100 $\mu mol \cdot m^{-2} \cdot s^{-1}$) at 22 °C, followed by 8 h of darkness at 22 °C.

7.2.2 *P. patens* transformation

7.2.2.1 Replication of plasmids in *E. coli* and their isolation

To obtain a sufficient quantity of recombinant plasmids for *P. patens* transformation, the provided plasmids were transformed into *E. coli*, and isolated from the cultivated bacterial cells.

OneShot™ TOP10 Chemically Competent *E. coli* cells were used for transformation. 25 µl of competent cells was thawed on ice, mixed with 1 µl of plasmid DNA (maximum 50 ng), and incubated for 10 min on ice. Heat shock was performed by placing the microtubes in a water bath preheated to 42 °C for 30 s and then immediately placed on ice. 125 µl of S.O.C. medium preheated to 37 °C was added and microtubes were incubated at 37 °C for 1 h at 200 rpm in a shaking incubator.

50 µl of the solution was spread onto plates containing LB medium with ampicillin or kanamycin (final concentration 50 $\mu g \cdot ml^{-1}$). The plates were sealed with the tape and incubated overnight at 37 °C. Randomly selected colonies were inoculated into 10 ml of liquid LB medium with ampicillin or kanamycin (final concentration 50 $\mu g \cdot ml^{-1}$). Cultures were incubated overnight at 37 °C at 200 rpm in a shaking incubator.

The plasmids were isolated from 4 ml of the bacterial culture using the GenElute™ Plasmid Miniprep Kit according to the protocol provided by the manufacturer.

7.2.2.2 Verification of the presence of insert

Two methods were utilised to check the presence of insert in the plasmid – PCR and restriction endonuclease digestion for *TR_KO* vector and *Cas9* vector, respectively.

PCR was conducted according to **section 7.2.9** using TR_KO downstream and TR_KO upstream primers. For digestion, 2 µl of rCutSmart buffer, 1.5 µl of plasmid, and 0.5 µl of *NotI_HF*

enzyme were mixed and filled with nuclease-free water to 20 µl. The plasmid was digested for 30 min at 37 °C.

The PCR and digested products were visualized by an agarose gel electrophoresis (**section 7.2.5**).

7.2.2.3 Transformation of *P. patens* protoplasts

P. patens protoplasts were transformed with a recombinant plasmid. The protoplast preparation and transformation were done according to Liu and Vidali (2011). Transformants were selected on medium supplemented by hygromycin to a final concentration 15 µg·ml^{-1}.

To achieve efficient transformation, the target fragment *TR_KO* plasmid was PCR amplified (**section 7.2.9**) using TR_KO downstream and TR_KO upstream primers. To maximise amplification efficiency, *TR_KO* plasmid was first linearised using the *SspI* restriction enzyme. The amplified *TR_KO* fragment was precipitated by $\frac{1}{10}$ volume of NaAc and 3 volumes of 96% ethanol and incubated for 3 h at –70 °C. Precipitated DNA was centrifuged for 15 min at 14 000 g at a room temperature. Pellet was washed with 75% ethanol, centrifuged for 5 min at 14 000 g at a room temperature, air-dried and dissolved in 20 µl of TE buffer. For transformation of *P. patens* protoplasts, 30 µg of *TR_KO* fragment DNA and 3 µg of *Cas9* plasmid DNA were used.

7.2.3 DNA isolation

For DNA isolation, the Dellaporta et al. (1983) protocol was supplemented by the phenol-chloroform-isoamyl alcohol extraction step to efficiently remove contaminants.

DNA concentration was assessed spectrophotometrically (**section 7.2.4**), and its integrity was verified by agarose gel electrophoresis (**section 7.2.5**).

7.2.4 Nucleic acids concentration and purity measurements

The concentration and purity of DNA were assessed spectrophotometrically using Nanodrop and fluorometrically using Qubit or TapeStation.

Spectrophotometric measurement of nucleic acids is based on the absorption of UV light by purine and pyrimidine bases of the nucleic acid, with an absorption maximum at 260 nm. Absorbance at this wavelength is directly proportional to nucleic acid concentration in the sample. Purity was verified by ratios of absorbance at wavelengths 260/280 nm for protein contaminants and 260/230 nm for organic compound contaminants.

For fluorometric assessment with Qubit, 3 µl of DNA was mixed with 197 µl of dsDNA BR working solution. DNA concentration measurement with TapeStation was performed according to the protocol provided by the manufacturer.

7.2.5 Nucleic acids agarose gel electrophoresis

Agarose gel electrophoresis was performed in 1× TAE buffer. The gel was prepared by boiling agarose (final concentration varies by method – see **Table 7.3**) and 1× TAE in a microwave oven. The solution was cooled to approximately 50 °C and ethidium bromide was added (final concentration 0.1 $\mu g \cdot ml^{-1}$). The gel was poured into a mould and left to solidify.

Samples for agarose gel electrophoresis were prepared differently depending on the type of analysis. 1 µl of DNA sample was mixed with 10 µl of sterile water for DNA integrity control. For the PETRA analysis, 1 µl of ubiquitin PCR product (prepared according to **section 7.2.9**) was mixed with 20 µl of two-step PCR product (**section 7.2.14**). For MNase digestion and TRF method, 20 µl of the samples were used.

DNA samples or 1 kb DNA ladder were mixed with 6× concentrated DNA loading buffer and loaded into the gel in an electrophoretic tank containing 1× TAE. Electrophoresis was performed according to the conditions in **Table 7.3**. DNA was visualized with Fusion Fx system.

Table 7.3 Conditions of agarose gel electrophoresis.

Method	Gel density	$V \cdot cm^{-1}$	Duration
DNA integrity control	0.8%	0.6 → 2.4	30 min → 30 min
TRF	1%	1.2	18 h
PETRA	1%	1.5 → 2.4	10 min → 3 h
MNase digestion	2%	0.6 → 1.8 → 2.4	30 min → 30 min → 3h

7.2.6 Nucleic acids alkaline agarose gel electrophoresis

Alkaline agarose gel electrophoresis was performed in alkaline electrophoresis buffer. The agarose gel was prepared by boiling agarose in alkaline gel buffer. The solidified gel was immersed in an alkaline electrophoresis buffer for 1 h.

DNA samples and 1kb DNA ladder were mixed with 6× concentrated alkaline DNA loading buffer and heated for 5 min at 70 °C and 95 °C, respectively, and chilled on ice for 3 min. The

electrophoresis was performed in a cold chamber (4 °C) for 18 h according to conditions listed in **Table 7.4**. Next, the gel was immersed in 0.5 M Tris-HCl for 30 min and was stained in a 0.5 μg·ml^{-1} ethidium bromide for 30 min. Non-specifically bound ethidium bromide was washed away for 10 min by 0.5 M Tris-HCl, and DNA was visualized with Fusion Fx system.

Table 7.4 Conditions of alkaline agarose gel electrophoresis.

Method	Gel density	V·cm^{-1}
PENT	1%	1.2
t-circle analysis	0.8%	2.0

7.2.7 Southern blot

DNA was transferred from the agarose gel to a positively charged nylon membrane (Roti® Nylon plus; pore size 0.45 μm; ROTH) using capillary blotting.

The agarose gel was incubated in 0.25 M HCl for 5 min to partially depurinate DNA. The gel was then rinsed with distilled water for 2 min. Subsequent DNA denaturation and fragmentation at depurinated sites was achieved by incubation in 0.4 M NaOH for 30 min. The nylon membrane was incubated in distilled water for 10 min.

The southern blot apparatus was assembled according to **Figure 7.1**. DNA fragments were transferred from an agarose gel to the nylon membrane overnight at a room temperature. The nylon membrane was washed in 2× SSC for 10 min and air-dried on a filter paper.

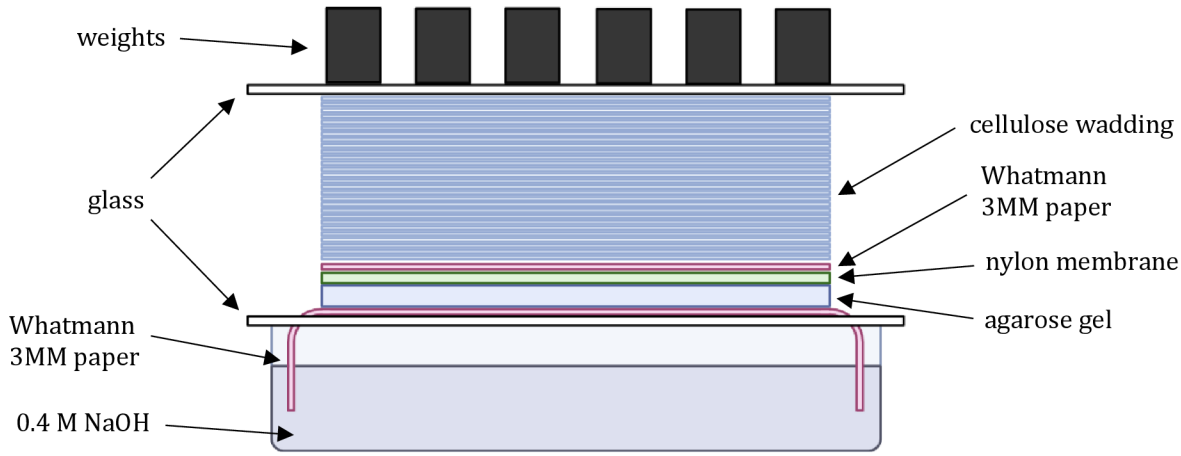

Figure 7.1 Scheme of Southern blot apparatus for transfer of DNA fragments from agarose gel to nylon membrane.

7.2.8 Dot blot

DNA dot blotting was performed according to the instructions provided by a manufacturer to a positively charged nylon membrane (Roti® Nylon plus; pore size 0.45 µm; ROTH). 200 ng, 40 ng, and 8 ng of DNA was blotted for ISiT detection.

Nylon membrane with bound DNA was hybridized with radioactively labelled telomere probe using random priming method (**section 7.2.10**). The probe for radioactive labelling was prepared by a PCR (**section 7.2.9**).

7.2.9 PCR

PCR was used to amplify (1) a fragment from *TR_KO* plasmid containing target region for *P. patens* transformation, (2) the ubiquitin 10 gene for the PETRA analysis, and (3) to prepare probe for ISiT detection.

The reaction mixture for ubiquitin 10 gene amplification consisted of MyTaq reaction buffer, primers (final concentrations 0.25 µM), MyTaq DNA polymerase (final concentration 25 $U \cdot ml^{-1}$), and 1 µl (approx. 50 ng) of DNA template (or sterile water as a negative control). As a template, genomic DNA isolated from *Arabidopsis thaliana* seedlings was used. The mixture was filled up to 20 µl with sterile water. For verifying the presence of insert in *TR_KO* vector and amplifying the *TR_KO* fragment, and for preparation of ISiT probe, DreamTaq reaction buffer was mixed with dNTPs (final concentration 0.25 mM each), primers (final concentrations 0.25 µM), DreamTaq DNA polymerase (final concentration 25 $U \cdot ml^{-1}$), and DNA template (linearised plasmid DNA, final concentration 1 $ng \cdot \mu l^{-1}$ and *P. patens* DNA, final concentration 2 $ng \cdot \mu l^{-1}$, respectively). Reaction without DNA served as negative control. The mixture was filled up with water to 20 µl.

PCR programmes are listed in **Table 7.5**.

Table 7.5 PCR programs. X stands for different annealing temperatures: 56 °C for ubiquitin, 55 °C for *TR_KO*, 57 °C for ISiT probe. Y stands for different durations of the primers extension: 30 s for ubiquitin and ISiT probe, 45 s for *TR_KO*. Steps repeated for 30 times are highlighted in grey.

Temperature	Duration	Process
95 °C	2 min	initial denaturation
95 °C	30 s	denaturation
X °C	30 s	annealing

Temperature	Duration	Process
72 °C	Y s	extension
72 °C	5 min	final extension

7.2.10 Radioactive labelling by random priming

7.2.10.1 Telomere probe preparation

Telomere probe was prepared using a non-template PCR protocol optimised according to Ijdo et al. (1991) and Adamusová et al. (2020).

For PCR reaction, 4 µl of 10 µM PlTelC and PlTeG primers were mixed with 20 µl of 5× concentrated MyTaq reaction buffer, 0.8 µl of 25 mM dNTPs, and 0.4 µl of MyTaq polymerase and filled with sterile water up to 100 µl. Reaction was performed according to **Table 7.6**.

Table 7.6 Non-template PCR program for telomere probe preparation. Steps repeated for 5 times and 25 times are in light grey and dark grey, respectively.

Temperature	Duration	Process
95 °C	3 min	initial denaturation
94 °C	1 min	denaturation
55 °C	30 s	complementary sequences annealing
72 °C	1 min	extension
94 °C	1 min	denaturation
60 °C	30 s	complementary sequences annealing
72 °C	90 s	extension
72 °C	5 min	final extension

7.2.10.2 Radioactive labelling of telomere probe by random priming

The telomere probe was labelled with a radioactive isotope by the random priming method using DecaLabel DNA labelling kit. As a radioactive compound, dATP with a ^{32}P-containing phosphate in the α-position was incorporated into DNA. The principle of random priming method is shown in **Figure 7.2**.

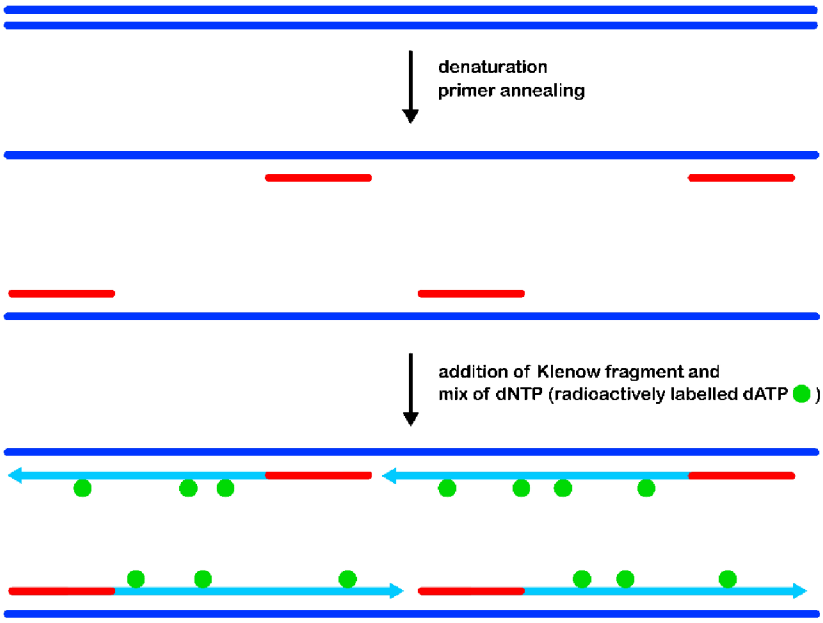

Figure 7.2 Radioactive labelling of the telomere probe by random priming method. DNA was heat denatured and primers (in red) were annealed. Primers were elongated using the Klenow fragment of DNA polymerase I and dNTP mix containing α-^{32}P-dATP (green dots).

Reaction mixture (total volume 40 µl) was composed of 25 µl of distilled water, 10 µl of reaction buffer containing a mixture of decanucleotides serving as random primers for DNA synthesis, and 5 µl (~100 ng) of plant telomere probe. The mixture was denatured for 10 min at 95 °C. After, 3 µl of MixA (mixture of dNTPs lacking dATP), 5 µl of α-^{32}P-dATP, and 1 µl of Klenow fragment were added to the reaction. Radioactive labelling was performed for 60 min at 37 °C. 5 min before the end of the reaction, 4 µl of complete dNTPs mix was added. Final denaturation occurred at 95 °C for 10 min.

7.2.10.3 DNA hybridization with telomere probe labelled by random priming

Prehybridization

1. Membrane was put into hybridization bottle and rinsed by 2× SSC.
2. Prehybridization was performed in 30 ml of hybridization solution for 1 h at 55 °C in a hybridization oven.

Hybridization

1. Hybridization solution was replaced with a fresh one and denatured radioactively labelled telomere prove was added.
2. The membrane was hybridized for 16 h at 55 °C in a hybridization oven.

Membrane washing

1. Hybridization solution was removed.
2. The membrane was washed twice for 5 min at 55 °C with washing solution I and twice for 10 min at 55 °C with washing solution II.
3. The membrane was rinsed with 2× SSC and distilled water, briefly dried on a filter paper and wrapped in a plastic foil.

The hybridization signal was detected according to **section 7.2.12**.

7.2.11 Radioactive end-labelling of telomere probe

7.2.11.1 Radioactive end-labelling of telomere probe

Radioactive end-labelling is based on the transfer of a radioactive phosphate (^{32}P) from the γ-position of ATP to the 5'-hydroxyl end of the oligonucleotide probe. Labelling reaction is catalysed by the T4-polynukleotide kinase (T4-PNK) enzyme.

PlTelG oligonucleotide was used as the template for radioactive end-labelling. 5 µl of 10 µM PlTelG, 2 µl of T4-PNK buffer, 5 µl of γ-^{32}P-dATP, and 1 µl of T4-PNK were mixed and filled up with distilled water to 20 µl. Radioactive labelling was performed at 37 °C for 1 h. Finally, the enzyme was inactivated at 95 °C for 2 min.

7.2.11.2 DNA hybridization with an end-labelled radioactive telomere probe

Prehybridization

1. Dried agarose gel was placed into a closable box and 40 ml of Denhardt's hybridization solution was added.
2. Prehybridization was performed for 1 h at 55 °C in a hybridization oven.

Hybridization

1. Denhardt's hybridization solution was replaced by a fresh one and end-labelled telomere probe was added.
2. The gel was hybridized over-night at 55 °C in a hybridization oven.

Membrane washing

1. The hybridization solution was discarded.
2. The gel was washed twice for 5 min at 55 °C with washing solution I and twice for 15 min with washing solution II.
3. The gel was rinsed with 2× SSC and distilled water and wrapped in a plastic foil.

Hybridization signal was detected according to **section 7.2.12**.

7.2.12 Detection of hybridization signals

A membrane or gel wrapped in a plastic foil was covered by a sensitive plate and embedded in a cartridge (FujiFilm).

The image, created by a radioactive signal corresponding to the position of telomeres at the membrane or gel, was scanned by the Typhoon FLA 9 500 phosphoimager (FujiFilm). Hybridization signals were evaluated using the WALTER programme (Lyčka et al., 2021).

7.2.13 TRF (terminal restriction fragments) analysis

The terminal restriction fragments (TRF) method was used to analyse the bulk telomere length. It is based on the digestion of genomic DNA by a frequently cutting restriction enzyme whose cleavage site is not located in the telomere repeat (Fojtová et al., 2015a). *MseI* restriction enzyme, which has a cleavage site `5′ T/TAA 3′`, was used.

5 000 ng of DNA was mixed with 2 µl of 10× rCutSmart buffer, 1 µl of *MseI* and filled up with sterile water to 20 µl (if the DNA concentration was low, total reaction volume was 30 µl). The mixture was incubated for 17 h at 37 °C. Then, 1 µl of *MseI* was added and incubation continued for 5 h at 37 °C. If necessary, the sample volume was reduced to 20 µl by lyophilisation.

Agarose gel electrophoresis (**section 7.2.5**) was performed. Separated DNA fragments were transferred to a nylon membrane using a Southern blot (**section 7.2.7**). The membrane

was hybridized with a radioactively labelled telomere probe prepared by a random priming method (**section 7.2.10**) and the hybridization signals were detected (**section 7.2.12**).

7.2.14 PETRA (primer extension telomere repeat amplification)

The length of telomeres on an individual chromosome arms was analysed by primer extension telomere repeat amplification (PETRA). The method is a PCR-based technique, comprising the binding of PETRA-T primer to telomere 3' G-overhang and its extension. Amplification of the extension product is enabled by the PETRA-A primer, complementary to the 5' region of the PETRA-T primer, and the subtelomere primer, which binds to the region near the telomere and is specific to respective chromosome arm. The principle of the PETRA protocol is illustrated in **Figure 7.3**.

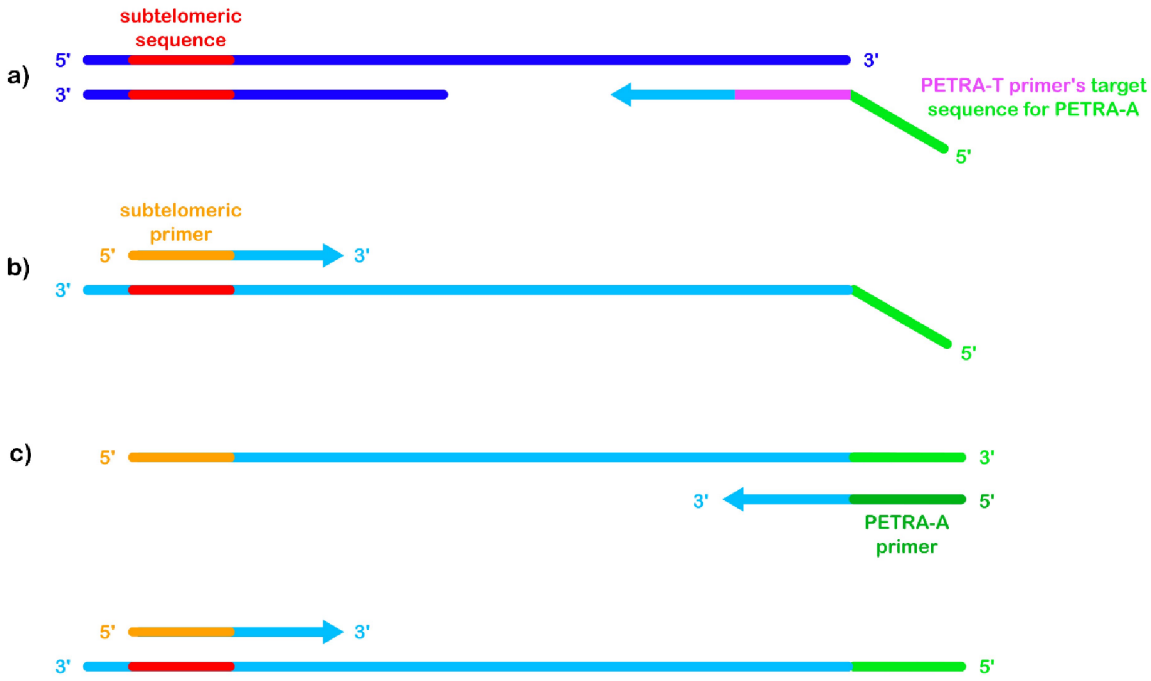

Figure 7.3 Schematic overview of PETRA workflow. **a)** PETRA-T primer containing complementary sequence for PETRA-A primer is annealed to the 3' G telomere overhang followed by its extension. **b)** Subtelomere primer binds to subtelomere sequence and complementary strand is synthesized. **c)** PETRA-A primer annealed to a complementary region at the 5' end of PETRA-T primer. Standard amplification of the extension product by PCR continues. Created by author according to Heacock et al. (2004).

Reaction mixtures and programmes are listed in **Tables 7.7 to 7.10**. PETRA products were separated by an agarose gel electrophoresis (**section 7.2.5**) with addition of 1 µl of ubiquitin PCR product (prepared according to **section 7.2.9**) to an electrophoretic mixture. DNA

was transferred to a nylon membrane by Southern blotting (**section 7.2.7**) and hybridized with a radioactively labelled telomere probe prepared by the random priming method (**section 7.2.10**).

Table 7.7 Reaction mixture for the first step of the PETRA analysis. Total reaction volume is 20 µl filled up with sterile water.

Component	Volume
DNA sample	500 ng
10× ExTaq buffer	2 µl
2.5 mM dNTPs	1 µl
10 µM PETRA-T primer	2 µl
ExTaq DNA polymerase	0.4 µl

Table 7.8 Conditions of the first step of the PETRA analysis.

Temperature	Duration	Process
65 °C	5 min	denaturation
55 °C	1 min	annealing
72 °C	10 min	extension

Table 7.9 Reaction mixture for the second PCR step of PETRA analysis. Total volume is 20 µl filled up with sterile water.

Component	Volume
Template from the 1st reaction	1 µl
10× ExTaq buffer	2 µl
2.5 mM dNTPs	1.6 µl
10 µM PETRA-A primer	0.5 µl
10 µM subtelomere primer	0.5 µl
DMSO	0.5 µl
ExTaq DNA polymerase	0.1 µl

Table 7.10 Conditions of the second PCR step of the PETRA analysis. Steps repeated for 20 times are grey highlighted.

Temperature	Duration	Process
96 °C	2 min	initial denaturation
96 °C	30 s	denaturation
60 °C	30 s	annealing
72 °C	2 min	extension
72 °C	5 min	final extension

7.2.15 PENT (primer extension nick translation)

Telomere 3' G-overhangs were analysed by the primer extension nick translation (PENT) method. The method is a PCR-based technique involving oligonucleotide annealing to a G-overhang and its elongation by nick translation. Scheme of the PENT reaction is illustrated in **Figure 7.4**.

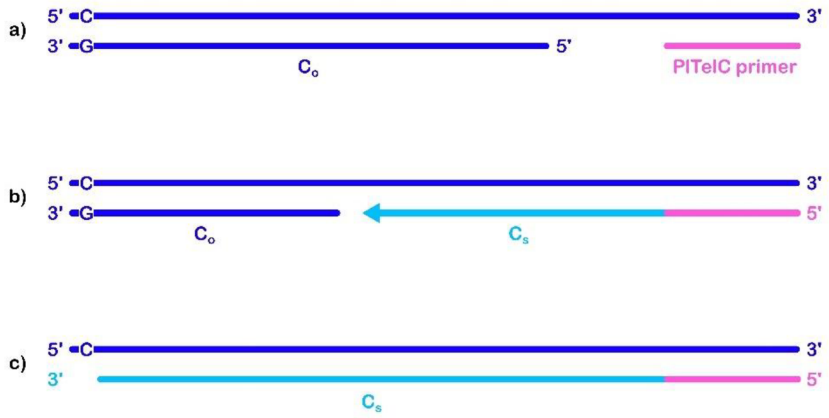

Figure 7.4 Scheme of the PENT reaction. **a)** PlTelC primer is annealed to the G-overhang. **b)** New telomere C-strand (C_s) is synthesized by the Taq polymerase. At the same time, the original C-strand (C_o) is degraded by 5' → 3' exonuclease activity of the Taq polymerase. **c)** In the absence of dGTP, C_s extension continues till the first cytosine in the template strand in the subtelomere region, where the reaction stops. Created by author according to Riha et al. (2000).

A modified version of the Riha et al. (2000) protocol was used. PENT reaction was performed in StandardTaq reaction buffer with PlTelC primer, and 2 µg of *P. patens* genomic DNA. Annealing of primer was conducted at 55 °C for 1 h. Subsequently, HotStartTaq DNA polymerase was added and the primer elongation continued at the same temperature for 1 h. Sample

was precipitated with 2.5 volume of ethanol, $\frac{1}{10}$ volume of 3 M NaAc, and 2 µl of GlucoBlue™ and dissolved in 20 µl of TE buffer.

PENT products were separated with alkaline agarose gel electrophoresis (**section 7.2.6**) and the gel was dried using Gel Drier. Dried gel was hybridized with radioactively end-labelled telomere probe (**section 7.2.11**).

7.2.16 Telomere circle (t-circle) assay

1000 ng of genomic DNA was mixed with 2.5 µl of 10× concentrated rCutSmart buffer, 0.5 µl of each restriction enzymes *RsaI* and *HinfI*, and filled with water up to 25 µl. Digestion was performed overnight at 37 °C. The next day, 0.5 µl of each restriction enzyme was added to a reaction and digested for another 4 h at 37 °C.

Samples were precipitated in $\frac{1}{10}$ volume of NaAc, 2.5 volumes of 96% ethanol, and 2 µl of GlycoBlue for 2 h at –20 °C, centrifuged for 15 min at 14 000 g at a room temperature, washed with 75% ethanol and air-dried. Precipitated DNA was dissolved in a) 20 µl of 10 mM Tris-HCl (pH 7.5) for reaction without primer (P-) or b) 18 µl of t-circle buffer and 2 µl of 10 µM ThioTel primer for reaction with primer (P+). P+ reaction underwent denaturation in a PCR cycler for 5 min at 96 °C, 120 min at 96–25 °C (gradual cooling by 0.6 °C – each temperature was held for 1 min), and 10 min at 25 °C. DNA from P+ reaction was precipitated under same conditions as before and dissolved in 20 µl of Tris-HCl (pH 7.5).

DNAs in both P+ and P- reactions were amplified by PCR using three variants of reaction mixture (for composition see **Table 7.11**): a) reaction with primer and with φ29-DNA polymerase; b) reaction without primer and with φ29-DNA polymerase; and c) reaction without primer and without φ29-DNA polymerase. t-circles amplification was carried out for 10 h at 30 °C and 20 min at 65 °C.

Table 7.11 Reaction mixture for t-circle PCR, total volume 20 µl. In case of reaction without φ29-DNA polymerase, sterile water was added instead of an enzyme.

Component	Volume
Sterile water	14.3 µl
10 mg·ml^{-1} BSA	0.5 µl
20% Tween	0.1 µl

Component	Volume
1 mM DTT	0.1 µl
25 mM dNTPs	1 µl
10× φ29-DNA polymerase buffer	2 µl
φ29-DNA polymerase (or sterile water)	1 µl
DNA (P+ or P- reaction)	1 µl

To detect the t-circles, the samples were separated using alkaline agarose gel electrophoresis (**section 7.2.6**), DNA fragments were transferred onto a nylon membrane (**section 7.2.7**) and hybridized with a radioactively labelled telomere probe (**section 7.2.11**).

Alternatively, amplified DNA reflecting presence of t-circles was analysed by qPCR. DNA was diluted four times with the TE buffer. The reaction mixture was prepared according to **Table 7.12**, and qPCR analysis was performed as listed in **Table 7.13**.

Table 7.12 Reaction mixture for t-circle qPCR, total volume 20 µl.

Component	Volume
Sterile water	7 µl
Elizyme mix	10 µl
10 µM TelA primer	1 µl
10 µM TelB primer	1 µl
4× diluted DNA (or sterile water)	1 µl

Table 7.13 Program for qPCR t-circle analysis. Steps repeated for 2 times and 20 times are light grey and dark grey highlighted, respectively.

Temperature	Duration	Process
95 °C	5 min	initial denaturation
94 °C	15 s	denaturation
49 °C	15 s	annealing
94 °C	15 s	denaturation
59 °C	10 s	annealing

Temperature	Duration	Process
74 °C	15 s	extension + fluorescence detection
74 °C	3 min	final extension
60–95 °C	–	melting curve analysis

C_T values were converted to relative changes in t-circles levels (R) by the $\Delta\Delta C_T$ method. Statistical evaluation was done using F-test followed by two-sample Student's t-test.

$$\Delta C_T = C_T(P^+\varphi^+) - C_T(P^-\varphi^-)$$

$$\Delta\Delta C_T = \Delta C_T(pptr) - \Delta C_T(wt)$$

$$R = 2^{-\Delta\Delta C_T} \cdot 100\ [\%]$$

$$\Delta SD = \sqrt{SD_{pptr}^2 + SD_{wt}^2}$$

$$max\ value = 2^{-\Delta\Delta C_T + \Delta SD} \cdot 100\ [\%]$$

$$min\ value = 2^{-\Delta\Delta C_T - \Delta SD} \cdot 100\ [\%]$$

7.2.17 Nuclei isolation and chromatin MNase digestion

300 mg of sample was ground in a chilled mortar using a chilled pestle, resuspended in 25 ml of nuclei isolation buffer and briefly vortexed. The suspension was incubated on ice for 15–20 min. Homogenized sample was filtered through a cheesecloth and the filtrate was centrifuged for 20 min at 11 000 g at 4 °C. The pellet was resuspended in nuclei isolation buffer and centrifuged under the same conditions.

The pellet, free from chloroplasts, was resuspended in 2 500 µl of nucleosome buffer and transferred to a new tube. The "empty" tube was centrifuged for 1 min at 11 000 g at 4 °C and the remaining pellet was resuspended in 500 µl of nucleosome buffer and add to the tube containing the rest of the suspension. The nuclei suspension was divided into five aliquots.

All the aliquots were incubated for 5 min at 1 200 rpm in thermoblock at 37 °C. Subsequently, 37.8 U·ml^{-1} of MNase was added to all the aliquots besides the undigested aliquot (0). The aliquots were incubated at 37 °C at 1 200 rpm for 1/3/5 or 10 min. Digestion was stopped by the addition of 1 volume of the STOP buffer.

The aliquots were mixed with RNase A (final concentration 80 µg·ml^{-1}) and incubated for 30 min at 37 °C. Subsequently, proteinase K (final concentration 160 µg·ml^{-1}) was added and

samples were incubated for 1 h at 52 °C. The DNA was extracted with 1 volume of phenol-chloroform-isoamylalcohol (25:24:1, v/v/v). The solution was centrifuged for 15 min at 14 000 g at a room temperature. The top aqueous phase containing DNA was mixed with 1 volume of chloroform-isoamylalcohol (24:1, v/v) following centrifugation under the same conditions. Top aqueous phase was collected and 0.6 volumes of isopropanol and 2 µl of Glycoblue were added for DNA precipitation. After 15 min incubation at a room temperature, the samples were centrifuged for 15 min at 14 000 g at a room temperature. The DNA pellet was air-dried and resuspended in 20 µl of TE buffer.

The DNA fragments were separated by agarose gel electrophoresis (**section 7.2.5**) and transferred onto a nylon membrane by a Southern blotting (**section 7.2.7**). The membrane was hybridized with radioactively labelled telomere probe prepared by the random priming method (**section 7.2.10**).

7.2.18 Isolation of telomerase extract

50–70 mg of *P. patens* tissue and *Arabidopsis thaliana* seedlings were homogenized using glass beads, mixed with 200 µl of W buffer and vortexed thoroughly. The suspension was centrifuged for 15 min at 20 000 g at 4 °C. The supernatant was transferred to a new microtube, mixed with 1 volume of 20% PEG 8000 and vortexed. The sample was rotated on a rotator for 30 min in a cold chamber (4 °C) to allow full dissolution. It was then centrifuged for 5 min at 20 000 g at 4 °C. The pellet was resuspended in 20 µl of buffer W and incubated for 30 min in a cold chamber on a rotator. Centrifugation was performed for 2 min at 25 000 g at 4 °C and the supernatant (telomerase extract, TEX) was transferred to a new microtube.

The protein concentration in the TEX was verified using Bradford method (**section 7.2.19**).

7.2.19 Protein concentration assessment

The protein concentration in the TEX was measured spectrophotometrically using Bradford method. 980 µl of the Bradford dye reagent was mixed with 16 µl of sterile water and 4 µl of TEX. Protein concentration in the sample was measured using spectrophotometer DU 730 (Beckman Coulter). If necessary, the water-sample ratio was adjusted to ensure that the protein concentration fell within the range of 0.1 $mg \cdot ml^{-1}$ and 0.5 $mg \cdot ml^{-1}$.

For TRAP (**section 7.2.20**), the TEX was diluted with W buffer to a final concentration 50 ng·µl^{-1} (T50) (*A. thaliana*) and 250 ng·µl^{-1} (T250) or 500 ng·µl^{-1} (T500) (*P. patens*).

7.2.20 TRAP (telomere repeat amplification protocol)

The TRAP is used to determine telomerase activity. In the first step of TRAP, the telomerase elongates a substrate primer. Following elongation, the telomerase is denatured and the DNA polymerase is activated. The elongated templates are amplified by PCR using a substrate primer and a reverse primer reflecting the sequence of synthesized telomere repeats. The TRAP principle is depicted in **Figure 7.5**.

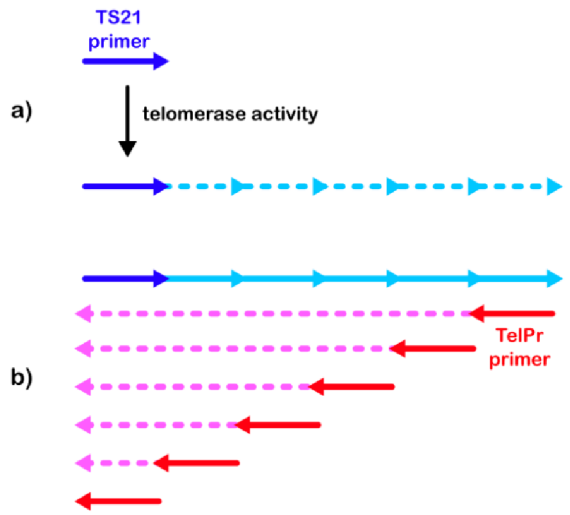

Figure 7.5 Schematic overview of TRAP. **a)** Substrate primer is extended by telomerase. **b)** Telomerase products are PCR amplified with reverse and substrate primers.

TRAP reaction mix was prepared according to **Table 7.14** and the reaction programme is listed in **Table 7.15**.

Table 7.14 Reaction mixture for the TRAP. Total volume is 25 µl, filled up with sterile water.

Component	Volume
5× Q5 buffer	5 µl
10 mM dNTPs	0.5 µl
10 µM substrate primer	0.5 µl
10 µM reverse primer	0.5 µl
Q5 HotStart polymerase	0.25 µl

Component	Volume
T50/T250/T500/W buffer	1 µl

Table 7.15 Conditions of the TRAP. X stands for different annealing temperatures: 60 °C for PpTelPr, 65 °C for TelPr. Steps repeated for 35 times are highlighted in grey.

Temperature	Duration	Process
26 °C	45 min	substrate primer elongation
95 °C	5 min	telomerase heat inactivation
94 °C	30 s	denaturation
X °C	30 s	annealing
72 °C	30 s	extension
72 °C	5 min	final extension

7.2.20.1 PAGE (polyacrylamide gel electrophoresis)

Products of the TRAP reaction were separated by PAGE. For a 12.5% polyacrylamide gel, 4 ml of 5× TBE was mixed with 12.5 ml of 40% AA:BIS (19:1), 40 µl of TEMED and 80 µl of 30% ammonium persulfate and filled to 40 ml with distilled water.

Samples for PAGE were mixed with 6× concentrated DNA loading buffer and loaded into the solidified vertical gel. The electrophoresis was performed in 0.5× TBE for 15 min at 170 V and 3 h at 300 V.

After electrophoresis, DNA was stained with GelStar fluorescent dye for 20 min. Signals were detected using Fusion Fx at SyberGREEN I detection channel.

8 Results

8.1 Plasmid PCR optimisation

To ensure successful *P. patens* transformation, the *TR* gene knock-out insert from the *TR_KO* recombinant plasmid was amplified by PCR. The reaction mixture consisted of MyTaq reaction buffer, primers (final concentrations 0.25 μM), MyTaq DNA polymerase (final concentration 25 $U \cdot ml^{-1}$), and DNA template (non-linearized plasmid DNA, final concentration 12.5 $ng \cdot \mu l^{-1}$). The PCR conditions were 95 °C – 2 min; 35 cycles at 95 °C – 30 s, 55 °C – 30 s, 72 °C – 30 s; and 72 °C 5 min. Unfortunately, the PCR was unsuccessful (results not shown), so the method had to be optimised first.

Optimisation was performed using PCR with non-linearized or linearized plasmids in five different concentrations. For plasmid linearization, the *SspI* restriction enzyme was used, as it has one cleavage site within the ampicillin resistance gene. PCR was performed with MyTaq DNA polymerase and two types of MyTaq reaction buffer (5× concentrated, containing Mg^{2+} ions and dNTPs; and 2× concentrated, containing Mg^{2+} ions, dNTPs and enzyme); and DreamTaq DNA polymerase and 10× concentrated DreamTaq buffer, containing only Mg^{2+} ions.

For the amplification of the *TR_KO* plasmid insert, a reaction with 10× concentrated DreamTaq buffer and a linearized plasmid in final concentration of 1 $ng \cdot \mu l^{-1}$ in the reaction mixture was chosen (**Figure 8.1**).

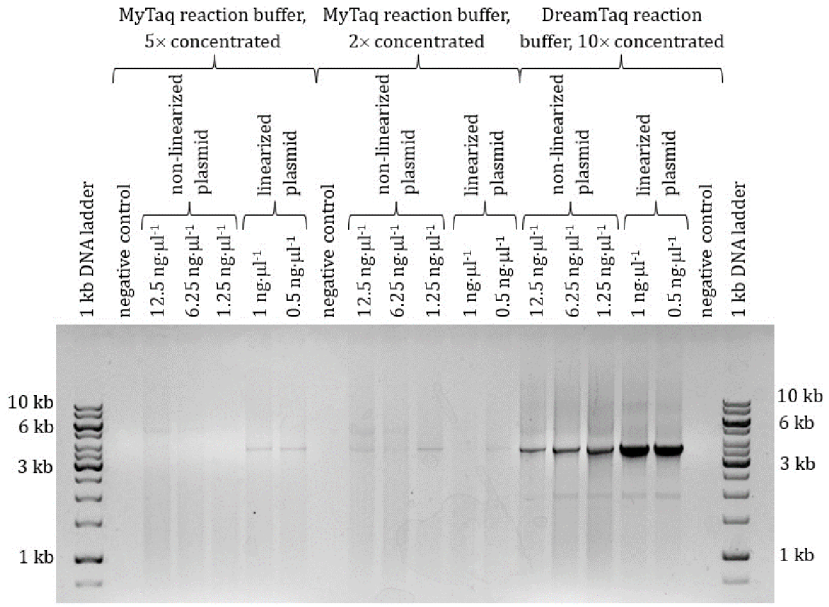

Figure 8.1 Plasmid PCR optimisation. Agarose gel electrophoresis of PCR products. Non-linearized and linearized (with *SspI* restriction enzyme) *TR_KO* plasmids were used as templates. Template concentration in the reaction and respective reaction buffers are depicted.

8.2 *P. patens* transformation

Protoplasts derived from *P. patens* protonema were transformed with *TR_KO* insert and *Cas9* plasmid. The transformed protoplasts were placed onto BCDAT medium (**section 7.2.1**) with 6% mannitol and cultivated under long-day conditions. After recovery, the transformed protoplasts should undergo selection on medium with addition of hygromycin. However, transformed protoplasts possessed bacteria contamination (**Figure 8.2**) and therefore, the cultivation was stopped.

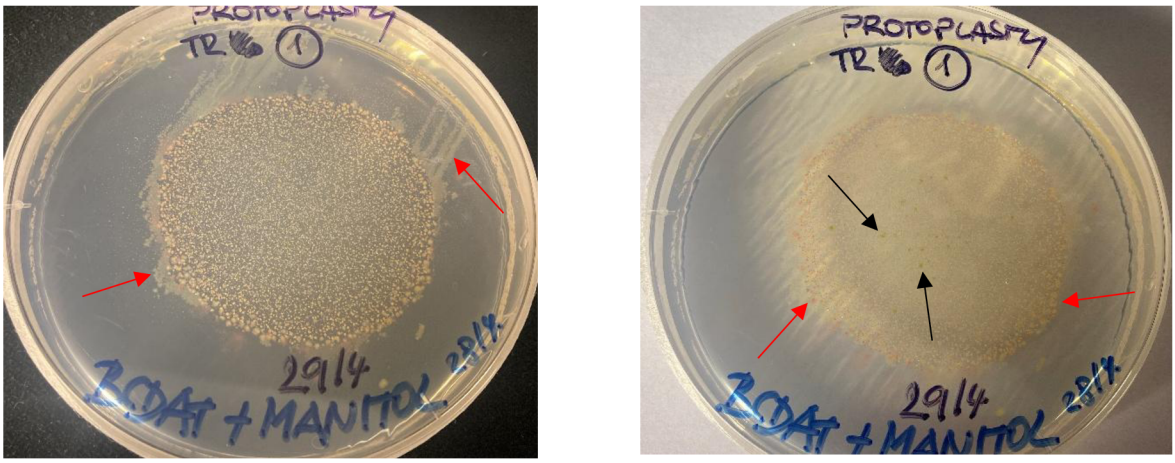

Figure 8.2 Transformed protoplasts cultivated on BCDAT medium with 6% mannitol. Red arrows point to bacteria contamination, black to regenerating protoplasts.

8.3 Analysis of the bulk telomere length in *pptr* mutants

In the previous research, significant changes in the telomere lengths and probably also in the structure of chromosome ends in *pptr* mutants were demonstrated (Fajkus et al., 2021). To find out if these changes are stable during prolonged cultivation of *pptr* culture, bulk telomere length was analysed using the TRF method with genomic DNA isolated from 7-day cultivated *P. patens* wild-type and *pptr* mutant cultures. Moss gametophytes were preserved in the form of very slowly growing cultures on the pure medium under low temperature (8–10 °C), then were homogenized and protonema cultures were cultivated under standard conditions (described in **section 7.2.1**) for 8–23 weeks.

The TRF results showed dramatic changes in telomere lengths and indicated probable changes of structure of telomeres in *pptr* mutant lines compared to the wild-type (**Figure 8.3**).

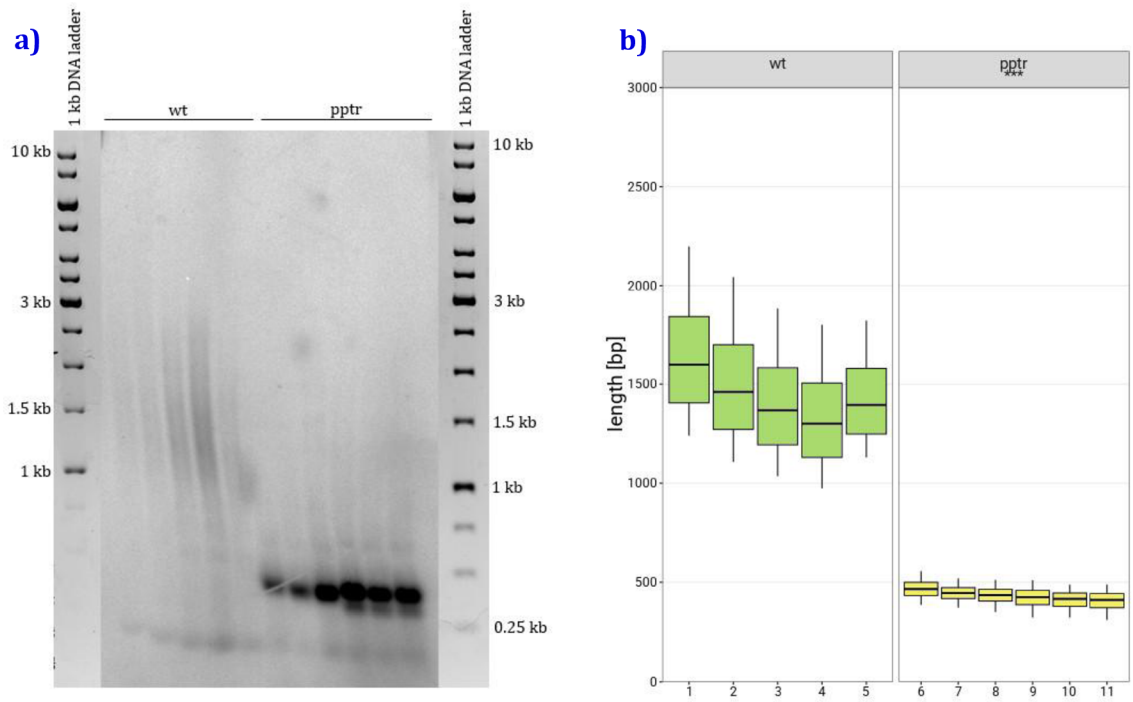

Figure 8.3 Bulk telomere lengths analysis using the TRF protocol in stable *pptr* mutant lines and *P. patens* wild-type (wt). **a)** DNA bound on nylon membrane was hybridized with radioactively labelled telomere probe. **b)** Evaluation of TRF hybridization profiles using the WALTER toolset. The statistics was calculate using Welch's t-test, $p < 0.01$ ***.

8.4 Analysis of telomere lengths on specific chromosome arms

8.4.1 PETRA optimisation

Telomeres at individual chromosome arms were analysed by the PETRA. First, the annealing temperatures of subtelomere primers were optimised. The optimal melting temperatures were assessed using the Tm Calculator (Thermo Fisher Scientific). Subsequently, PCR was conducted with a $T_A = 60$ °C and cycles repeated for 20 times for all primers (**Figure 8.4 a**). Primer 21L was crossed out from further optimisations because it did not give a rise to any telomere-specific signal.

Next, the number of cycles used for telomere amplification was optimised, conditions selected for further analyses are presented (**Figure 8.4 b**). The number of cycles was not optimised for primer 21R since the initial 20 cycles was optimal. From other use, primer 9L was crossed out because it did not give a rise to any telomere-specific signal.

Optimized primers used for analyses of telomere lengths on specific chromosome arms include 2R, 3L, 10L, 21R, 24L, and 24R.

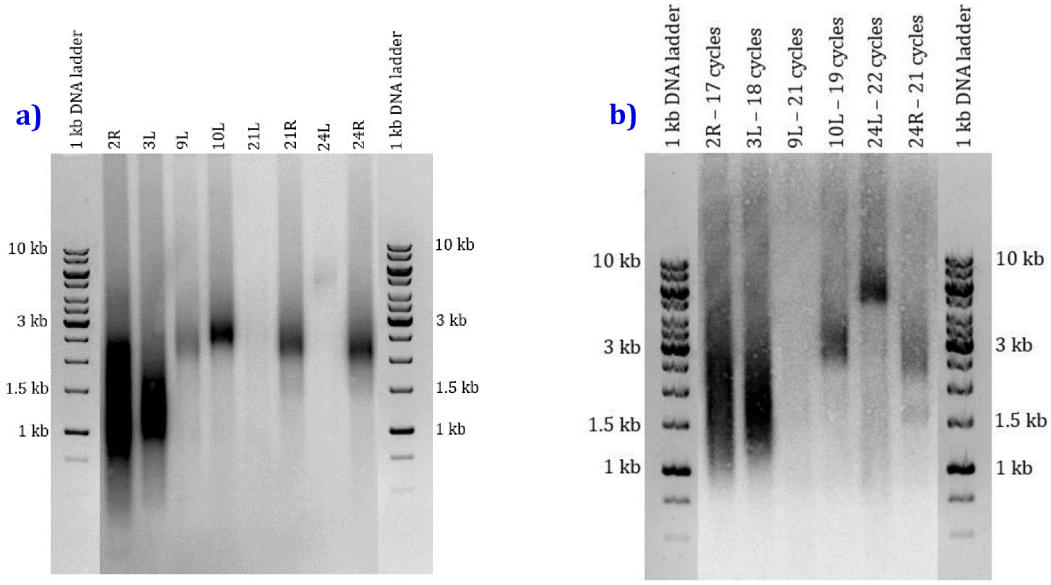

Figure 8.4 Optimisation of PETRA. **a)** Results of PETRA using different subtelomere primers and annealing temperature– 60 °C. **b)** Optimised numbers of PCR cycles for PETRA using respective subtelomere primers.

8.4.2 Telomeres in *pptr* mutants

We aimed to assess telomeres in ALT *pptr* lines at individual chromosome arms. Telomere lengths on chromosome arms 2R, 3L, 10L, 21R, 24L, and 24R were analysed using the PETRA method with genomic DNA isolated from 7-day cultivated *P. patens* wild-type and *pptr* mutant lines.

Detection of telomeres in the *pptr* mutant lines failed in all analyses, indicating important structural changes at chromosome ends in the *P. patens* mutant lines (**Figure 8.5**).

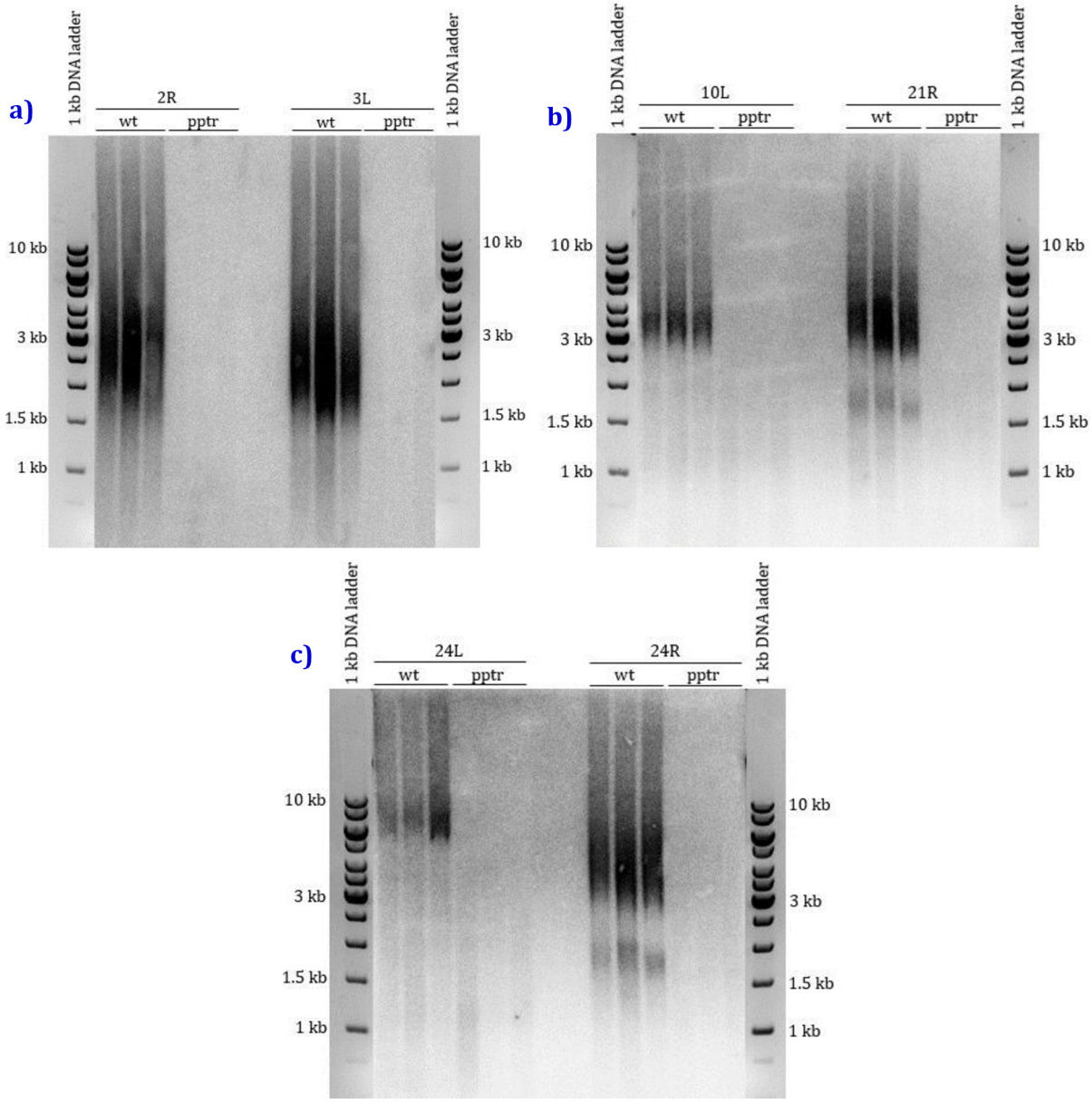

Figure 8.5 PETRA analysis of telomere lengths at **a)** 2R, 3L, **b)** 10L, 21R, **c)** 24L, and 24R chromosome arms in stable *pptr* mutants and wild-type moss (wt). DNA bound on nylon membrane was hybridized with radioactively labelled telomere probe.

8.5 Analysis of the telomere chromatin structure

8.5.1 Optimisation of MNase chromatin digestion

Two different approaches were used for nuclei isolation. The first approach used a nuclei isolation buffer and is described in **section 7.2.17**. The other approach was based on Percoll nuclei isolation (Sikorskaite et al., 2013). For further analyses, the nuclei isolation buffer protocol was selected, since it yielded more DNA from the same amount of wild-type moss culture (**Figure 8.6**, lines 0').

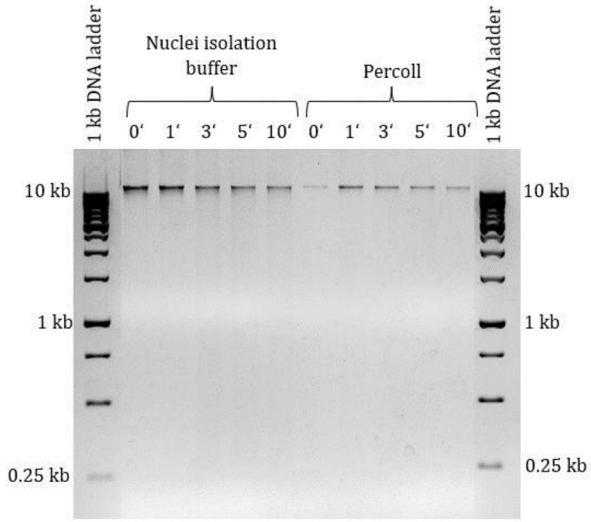

Figure 8.6 Selection of extraction buffer for nuclei isolation. The agarose gel electrophoresis of DNA isolated from chromatin. Chromatin was isolated from wild-type *P. patens*.

Next, the MNase digestion conditions were optimised. Digestion was performed with regular shaking at 1 200 rpm (MNase digestion of chromatin without shaking was not successful, **Figure 8.6**). Furthermore, the digestion buffer was optimised. Two types of buffer were tested for nuclei digestion by MNase – nucleosome buffer (see **section 7.1.3** for composition) and MNase digestion buffer (20 mM HEPES (pH 7.5), 50 mM NaCl, 0.5 mM DTT, 0.5% NP-40 Nonidet, 3 mM $CaCl_2$, 0.5% Triton-X, 0.2 mM PMSF, 4 $\mu g \cdot ml^{-1}$ leupeptin, 2 $\mu g \cdot ml^{-1}$ pepstatin). The nucleosome buffer was chosen for further use due to the better digestion pattern (**Figure 8.7**).

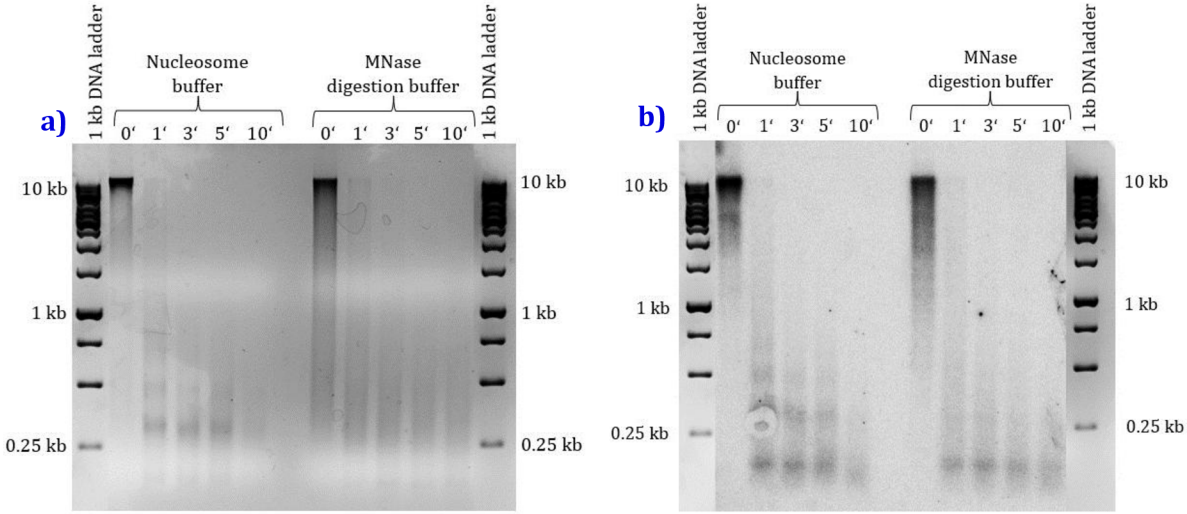

Figure 8.7 Optimisation of buffer for chromatin MNase digestion. **a)** The agarose gel electrophoresis of DNA isolated from digested chromatin isolated from wild-type *P. patens*. **b)** Hybridization of DNA isolated from digested chromatin with radioactively labelled telomere probe. Times of MNase digestion in min are depicted.

Finally, the amount of MNase for chromatin digestion was optimised. Previous reactions were carried out using 150 U·ml^{-1} of MNase. This relatively high amount of an enzyme mostly led to the blurring of the typical oligonucleosome-reflecting pattern of DNA isolated from digested chromatin. Therefore, the amount of a MNase enzyme was reduced to75 U·ml^{-1} and to 37.8 U·ml^{-1}.

The best digestion pattern was observed with the lowest enzyme concentration (**Figure 8.8**). Therefore, a final MNase concentration of 37.8 U·ml^{-1} was chosen for further experiments.

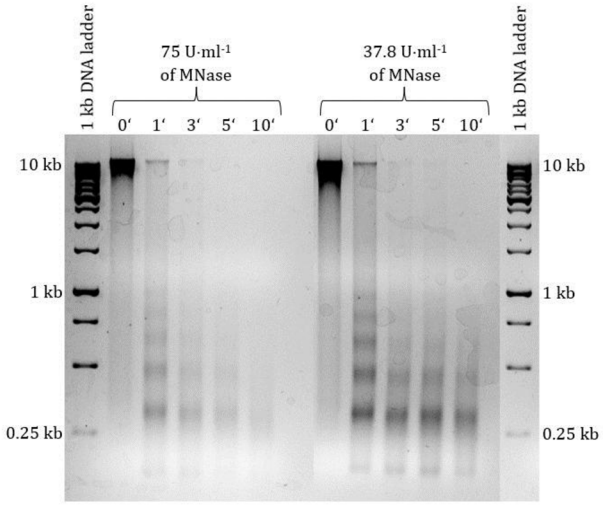

Figure 8.8 Optimisation of the amount of MNase for chromatin digestion. Ethidium bromide-stained agarose gel electrophoresis of DNA isolated from nuclei isolated from wild-type *P.patens* digested by MNase. Times of MNase digestion in min are depicted.

8.5.2 Telomere chromatin in *pptr* mutants

Based on the presented (**Figure 8.3** and **Figure 8.5**) and previously published data (Fajkus et al., 2021) the structure of the telomere chromatin in *pptr* lines seems to be significantly different compared to the *P. patens* wild-type. Thus, we performed the basics analysis of the chromatin structure and the bulk and telomere chromatin were analysed via MNase digestion. Nuclei were isolated from 7-day cultivated *P. patens* wild-type and *pptr* mutant lines and DNA was isolated following MNase digestion.

Generally, no changes in the structure of either bulk or telomere chromatin structure – in terms of accessibility to MNase – were observed between the wild-type and mutant lines (**Figure 8.9**). However, evaluation of results was rather complicated by significant differences in the DNA yields from *pptr* and wild-type samples (despite of that nuclei were isolated from the same amounts of material).

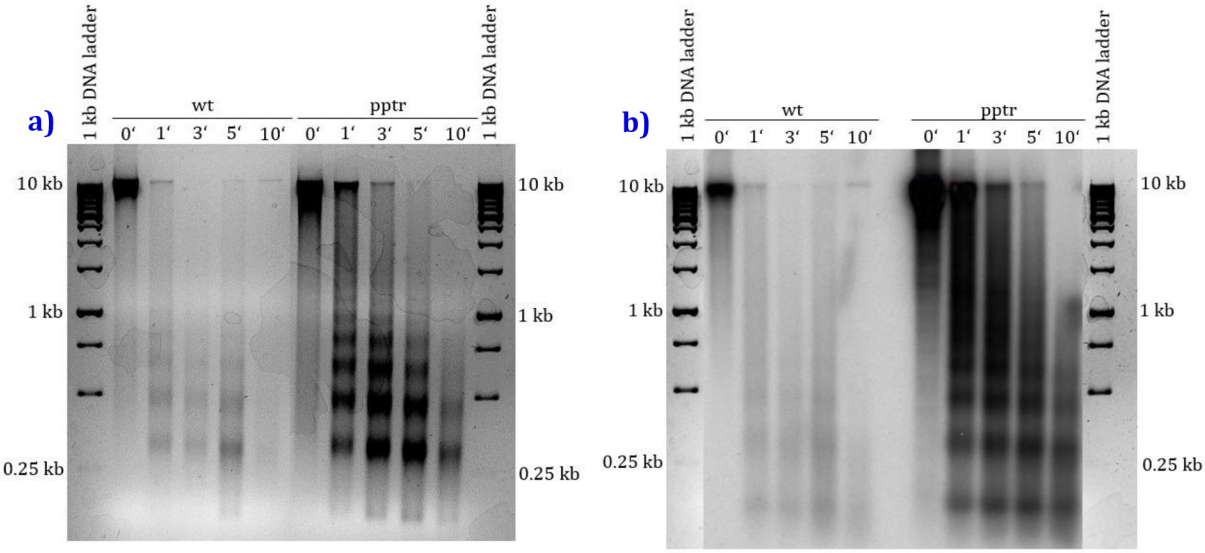

Figure 8.9 Analysis of the bulk and telomere chromatin structures in *pptr* mutant and wild-type (wt) lines. **a)** Ethidium bromide-stained agarose gel electrophoresis of DNA isolated from nuclei digested by MNase; **b)** DNA on nylon membrane hybridized with radioactively labelled telomere probe showing structure of telomere chromatin. Times of MNase digestion in min are depicted.

8.6 Analysis of telomere G-overhangs

8.6.1 Optimisation of methods for G-overhangs analysis

The results of the PETRA indicated absence of G-overhangs in *pptr* mutants, as these overhangs are essential for the first step of PETRA protocol, annealing of the PETRA-T primer (**Figure 7.3**). To confirm this hypothesis, two additional methods were tested for the detection of telomere G-overhangs: in-gel hybridization and the PENT analysis. In-gel hybridization was conducted according to the protocol in **Appendix A**. However, optimisation of the in-gel hybridization was not successful, any telomere-specific hybridization signal was obtained neither in the line with *A. thaliana* DNA serving as a positive control (**Figure A.1**). The PENT reaction was therefore conducted instead.

For PENT, the annealing and elongation temperatures were optimised. 2 µg of *P. patens* DNA were used for the PENT reaction. *Arabidopsis thaliana* DNA was used as a positive control to test the functionality of the method. For further research, 65 °C was chosen as the annealing and likewise elongation temperatures (**Figure 8.10**). Nevertheless, surprisingly and rather unexpectedly, there was no hybridization signal detected in the *P. patens* TRF line and the lengths

of PENTA products were comparable for both species tested despite of different telomere lengths (~ 3 kb in *A. thaliana*, ~ 1.5 kb in *P. patens*).

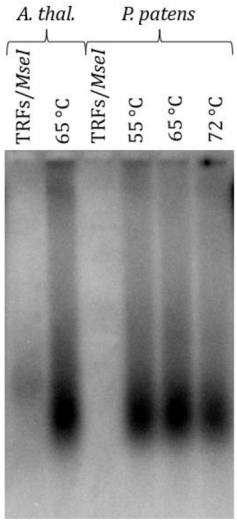

Figure 8.10 Optimisation of annealing and elongation temperatures for the PENT reaction. Hybridization of PENT products with radioactively labelled telomere probe is presented. As a length control, TRFs were used.

To deal with this problem, different DNA polymerases and the durations of elongation steps were tested. Final concentration of HotStartTaq polymerase in reaction mixture was 40 U·ml^{-1}, and 100 U·ml^{-1} for φ29-DNA polymerase and DNA polymerase I. The φ29-DNA polymerase was denatured after elongation for 5 min at 95 °C.

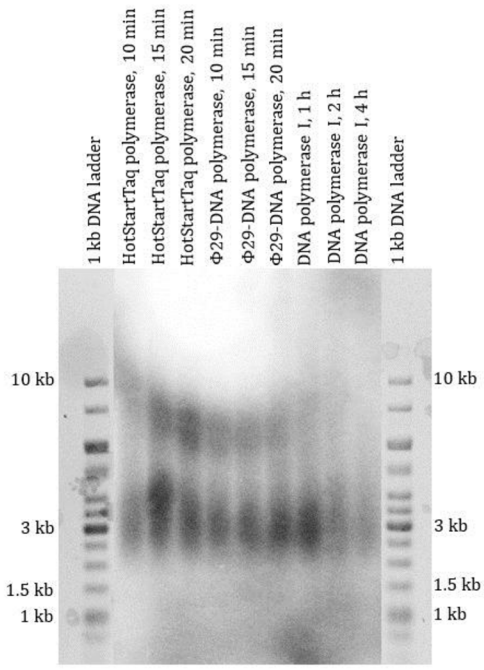

Figure 8.11 Optimisation of the elongation step and DNA polymerase for the PENT. Hybridization of PENT products with radioactively labelled telomere probe is presented.

The results from all reactions appeared in same way – the C_s telomere fragments lengths were around 3 kb (**Figure 8.11**). Since the reaction mix lacked dGTP, the elongation should stop at the first cytosine, i.e., probably very close to the genuine telomeres. Thus, either PENT does not work as expected or the first cytosine in subtelomere regions of the G-rich strands occurs much further from the telomeres than expected.

For further analysis, HotStartTaq polymerase was chosen, with an annealing and subsequent elongation temperature at 55 °C and an elongation step duration of 1 h, since this combination produced the strongest signal (**Figure 8.11**).

8.6.2 Telomere G-overhangs in *pptr* mutants

Genomic DNA isolated from 7-day cultivated *P. patens* wild-type and *pptr* mutant lines was analysed by the PENT method.

Surprisingly, PENT analysis revealed no differences in the hybridization signals between the telomeres of the wild-type and *pptr* mutant lines (**Figure 8.12**). Nevertheless, in all analyses, the telomere fragments in *P. patens* samples were significantly longer than expected. At

least in wild-type *P. patens* samples, PENTA hybridization signal was supposed to co-localize with the TRF hybridization signal, ~ 1.5 kb.

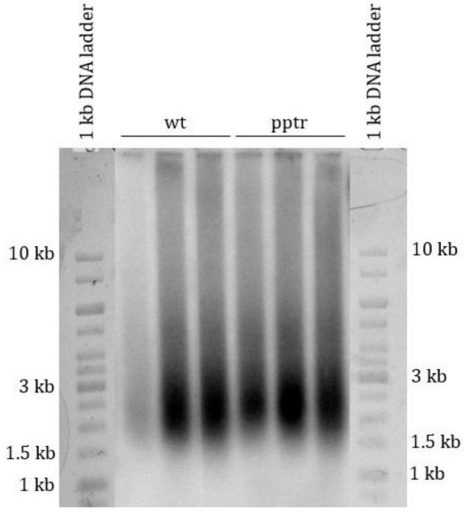

Figure 8.12 Telomere G-overhangs analysis in *pptr* mutant and wild-type (wt) lines using the PENT method.

8.7 Analysis of ISiT (interstitial sequence within telomeres)

A specific subtelomere sequence, amplified and spread across whole genome, especially into telomeres, was identified in *pptr* mutants based on preliminary results of Nanopore sequencing analysed by Mgr. Petr Fajkus, Ph.D. from Institute of Biophysics, CAS, Brno.

To verify this observation, dot blot analysis of the ISiT was performed. The DNA of three wild-type and three *pptr* mutant samples isolated from 7-day-cultivated cultures was loaded onto a nylon membrane in three final concentrations (200 ng, 40 ng, and 8 ng) and hybridized with radioactively labelled part of the ISiT amplified by PCR.

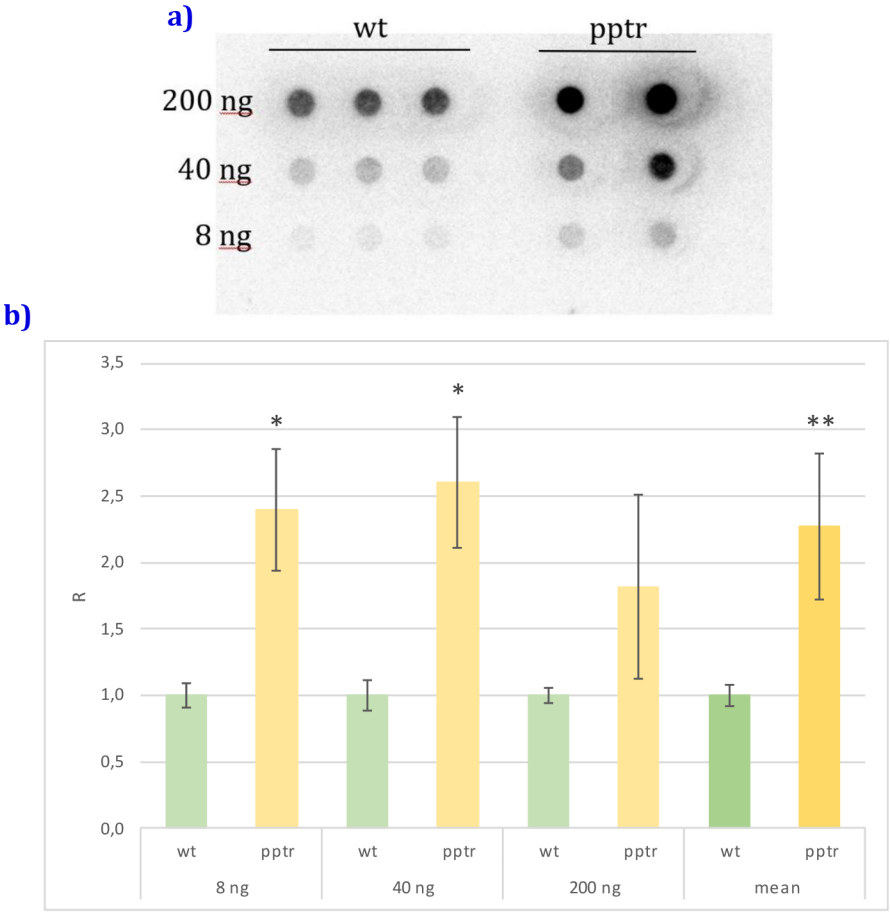

Figure 8.13 Dotblot analysis of ISiT. Three concentrations of DNAs were loaded onto a nylon membrane (200 ng, 40 ng, and 8 ng) and hybridized with the radioactively labelled ISiT probe. **a)** DNA on nylon membrane hybridized with ISiT probe. **b)** Hybridization signal intensities in *pptr* mutant line and wild-type (wt). *R* – relative hybridization signal intensity, R in wt samples has been arbitrarily chosen as 1; $p < 0.05$ *, and $p < 0.01$ **. 2–3 biological replicates were analysed.

The results show higher ISiT-specific hybridization signals in *pptr* mutants compared to wild-type (evaluated using MultiGauge tool), indicating elevated level of ISiT in mutant moss (**Figure 8.13**), supporting the results from the Nanopore sequencing.

8.8 t-circle analysis

8.8.1 Optimisation of t-circles analysis

The t-circles in *pptr* mutant lines were quantified using qPCR. DNA isolated form *A. thaliana ku70* mutant was used as a positive control, as telomeres in this line are elongated using the

ALT mechanism (Sováková et al., 2018). However, despite numerous optimizations, our results were not consistent with previous observations, indicating problems with the method and suggesting that further optimisations are needed (**Figure 8.14**).

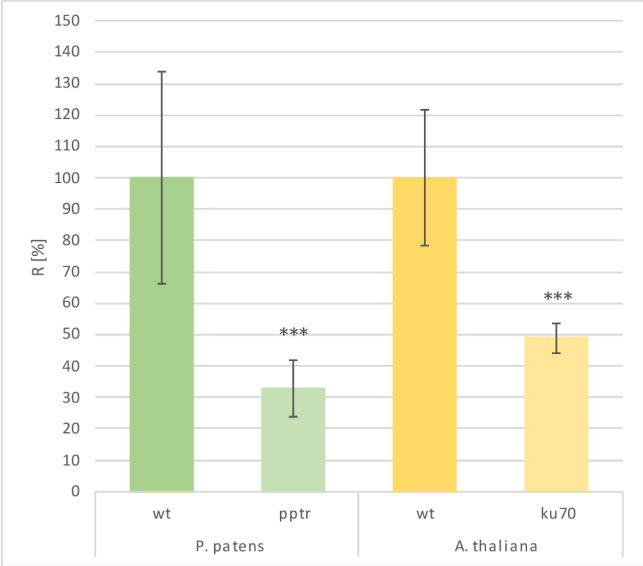

Figure 8.14 t-circle quantification pilot results in stable pptr mutant line and wild-type (wt). *A. thaliana ku70* mutant was used as positive control. *R* – t-circles level in % relatively to wt plants; $p < 0.001$ ***. 2 biological replicates were analysed.

Possible explanation for these unexpected results may lay in the existence of more types of extrachromosomal telomere DNA – t-circles (double stranded circles) or single stranded C- or G- circles (C- or G-rich telomere strand, respectively) (Cesare and Reddel, 2010). Used method enables detection of t-circles through rolling circle amplification of ThioTel primer. Its C-rich sequence annealed to complementary G-rich strand of t-circles or single strand G-circles. However, the most abundant type of circles in the ALT – C-circles – cannot be detected using this primer. On the other hand, at least for *A. thaliana ku70* mutants, if the method was working correctly, we should obtain same data as in many previous experiments, i. e., a significantly stronger signal compared to wild-type.

Nevertheless, an analysis with the primer with G-rich sequence (PlTelG) for rolling circle amplification of extrachromosomal circles step was performed to detect the possible presence of C-circles. Quantification of C-circles in *pptr* mutants compared to wild-type showed promising path for further research since its level was elevated. Nevertheless, in *A. thaliana* wild-type and *ku70* mutant, the levels were comparable (**Figure 8.15**).

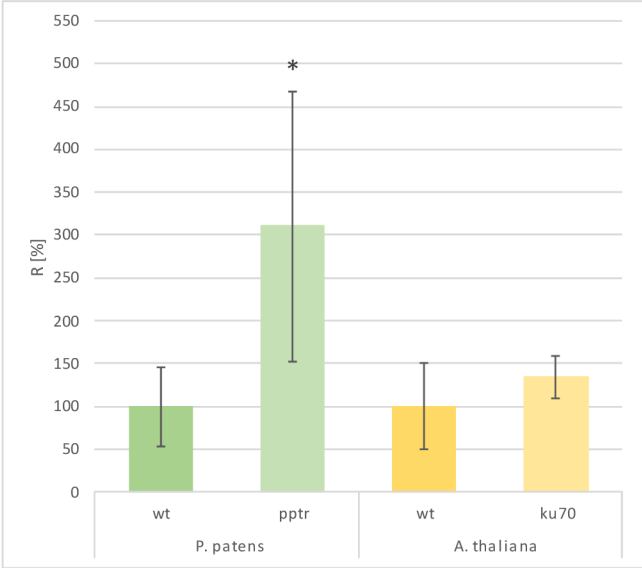

Figure 8.15 C-circles quantification in *pptr* mutant line and wild-type (wt). *A. thaliana ku70* mutant was used as positive control. *R* – C-circles level in % relatively to wt plants; $p < 0.05$ *. 2 biological replicates were analysed.

8.9 Analysis of telomerase activity

8.9.1 Optimisation of TRAP

Ten combinations of substrate primers (47F, CAMV, PpTS, PpTS2, and TS21), and reverse primers (PpTelPr, and TelPr) was tested to find functional pair for *P. patens*. Telomerase extract isolated from 7-day-old *A. thaliana* seedlings served as a positive control (**Figure 8.16**).

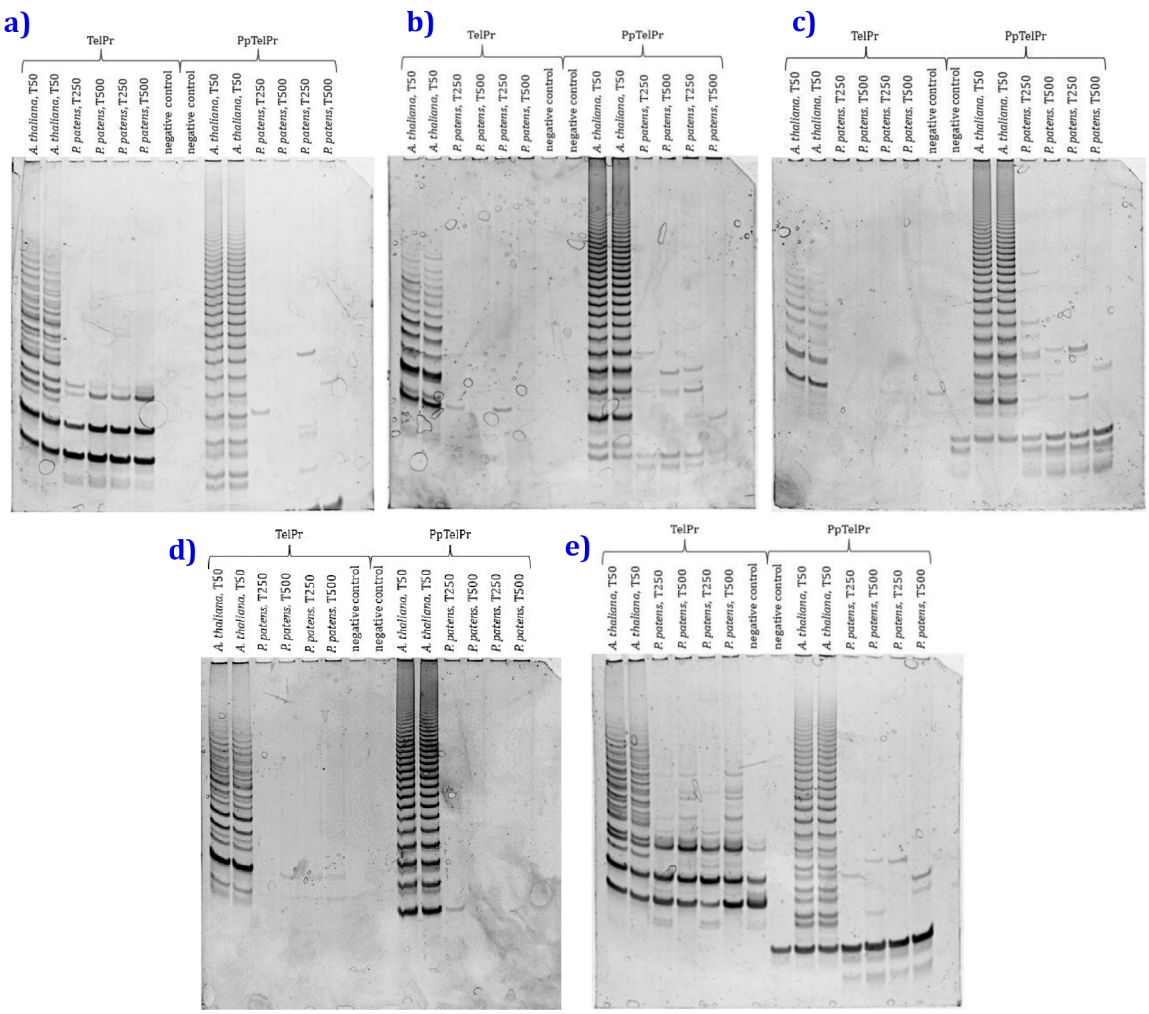

Figure 8.16 TRAP optimisation of primers combination results. TEX isolated from 7-day-old *A. thaliana* seedlings and diluted to T50 was used as a positive control. TEX isolated from *P. patens* was diluted to T250 and T500. Each TEX was isolated in duplicates. Reverse primers (TelPr, PpTelPr) were combined with **a)** TS21, **b)** PpTS, **c)** PpTS2, **d)** CAMV, or **e)** 47F substrate primer.

Promising primer pair for further analyses is TelPr and TS21 (**Figure 8.16 a**), since it is the only pair which is functional and did not create a signal in negative control such as TelPr and 47F primer pair (**Figure 8.16 e**), although it may be a technical issue. However, TelPr in combination with 47F and *P. patens* T500 create better "ladder" more similar to the one from *A. thaliana* T50 (**Figure 8.16 e**). In further experiments, it would worth to reduce the non-specific reaction by optimizing the composition of reaction solution, e.g., adding the DMSO.

For telomerase activity analysis in this thesis, primer pair TelPr and TS21 with *P. patens* T500 was used (**Figure 8.16 a**).

8.9.2 Telomerase activity in *pptr* mutants

Since the *pptr* mutants are supposed to lack the telomerase activity (Fajkus et al., 2021), we performed the analysis of telomerase activity in wild-type and *pptr* mutant lines using the TRAP method. The activity was measured with TEX diluted to T500 in case of *P. patens* or to T50 for *A. thaliana*, which was used as positive control.

Results of telomerase activity analysis did not show any differences between wild-type and *pptr* mutants (**Figure 8.17**).

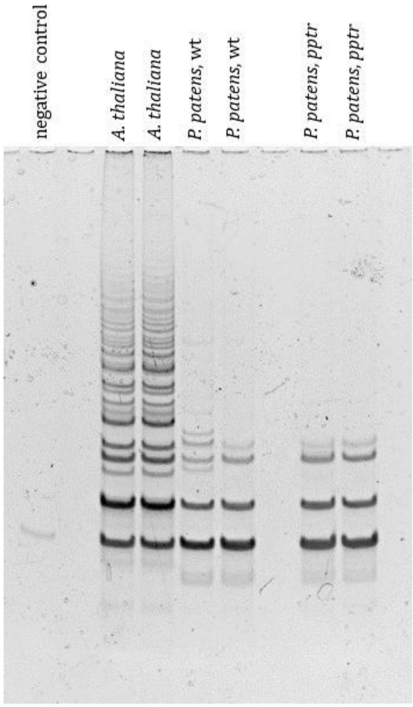

Figure 8.17 Analysis of telomerase activity in *pptr* mutants and wild-type (wt) by the TRAP.

9 Discussion

Telomeres compensate the disability of DNA polymerase to synthesizes the chromosome very ends and therefore are involved in the solution of the end-replication problem. Telomeres shorten every cell cycle and hence function as marker for cellular senescence. In some cases, – such as in human stem cells or in proliferating meristematic cells in plants – telomere shortening is an unwanted effect. Therefore, telomeres can be elongated by a nucleoprotein complex, telomerase. Beside telomerase, telomere maintenance can be ensured by telomerase-independent mechanism, ALT. It is a mechanism based on HR, using mainly other telomeres as a template for telomere elongation.

ALT is typically activated in 10–15% of cancer cells or in organisms that are defective in telomerase, e.g., TERT mutant of *A. thaliana* (Růčková et al., 2008) or *Caenorhabditis elegans* (Meier et al., 2006). ALT was detected in *P. patens* TR knock-out mutant. *pptr* mutants, which were used for all analyses in this thesis, are stable during long-term cultivation. These mutants were generated and selected in a pilot study Fajkus et al. (2021). In this study, TRF analysis showed significant changes in telomere-specific hybridization signal in *pptr* plants compared to wild-type.

These findings were in accordance with results of TRF analysis performed in this thesis. We analysed stable *pptr* mutant line, which was maintained as slowly growing gametophytes. Following homogenization, protonema were formed and cultivated for 8–23 weeks. The bulk telomere length was in wild-type plants assessed to approximately 1.5 kb, and to 400 bp in *pptr* mutant (**Figure 8.3**). This observation is consistent with previously reported changes of telomere lengths in ALT cell lines which was preserved during long-term maintenance of *pptr* line. Despite comparable DNA loading in all lines of the agarose gel, the intensity of telom

ere-specific hybridization signal was consistently several times higher in *pptr* mutants compared to wild-type samples. Furthermore, the telomere-specific hybridization signal derived from *pptr* mutants was notably more compact than diffuse signal from wild-type plants (**Figure 8.3 a**). Higher telomere signal compactness can be caused by structural rearrangements of telomeres elongated by telomerase-independent mechanism, such as spreading of subtelomere sequences into telomere region or higher mutant rate and therefore increased content of TVRs. These events would lead to the *de novo* formation of cleavage sites for *MseI* restriction enzyme, which was used for DNA digestion in the first step of the TRF analysis

(**section 7.2.13**). Higher signal intensity could also signify an elevated content of telomere repeats in *pptr* mutant compared to wild-type. These repeats are separated by non-telomere sequences digestible by *MseI*, thus it did not manifest as telomere elongation.

The results of TRF analysis could also indicate changes in the telomere chromatin structure. For cells with activated ALT mechanism, it is typical to have looser telomere chromatin than cells which telomeres are elongated by telomerase. This phenotype is caused by the absence or mutation of chromatin remodelling complexes in ALT cell lines (reviewed O'Sullivan and Greenberg, 2025). To test the hypothesis, chromatin structure in *pptr* mutants was analysed by MNase digestion. Since MNase is an enzyme, which digests free DNA, i. e., DNA which isn't structured within nucleosomes, higher digestion frequency was expected in case of less dense chromatin. However, no significant changes of chromatin structure between wild-type moss and *pptr* mutants were detected neither at the level of bulk chromatin nor telomere chromatin (**Figure 8.9**). It is necessary to stress, that in comparison with other approaches for analysis of the chromatin structure, e. g., ATACseq, the MNase is insufficient to distinguish even between heterochromatin and euchromatin (Mansisidor and Risca, 2022; Schwartz et al., 2019). Hence, other approaches, e. g., ATACseq, will be used in the future analyses of telomere chromatin strucutre in *pptr* mutants.

The interesting phenomenon observed in the analysis of telomere chromatin strucutre was different signal intensity in *pptr* samples in both bulk chromatin and telomere chromatin analyses (**Figure 8.9**). Interestingly, it is similar to the TRF results (**Figure 8.3 a**). Except of hypothesis presented above, next probable explanation lies in *pptr* mutant phenotype. During cultivation, mutant moss shows retarded growth which could lead to higher number of smaller cells per square. To test this hypothesis, time resolved microscopic analysis of cultivated protonema will be conducted in the future.

Telomere lengths on specific chromosome arms were measured using PETRA method. We were not able to detect telomere-specific hybridization signal in *pptr* mutants in all tested chromosome arms indicating changes in telomere structure (**Figure 8.5**). The most probable is the loss of telomere 3' G-overhang. It came out of the principle of PETRA method which use two steps for telomere amplification. In the first step, PETRA-T primer anneals to a G-overhang and is extended. This product served as a template for amplification by PCR (for details see **section 7.2.14**). Therefore, in the absence of G-overhangs, there is no place for PETRA-T annealing and the subsequent elongation cannot be proceed. This leads to missing template for

the second step of PETRA reaction resulting in missing signal on membrane with bound DNA and hybridized with telomere specific radioactively labelled probe.

For further research, we plan to detect telomere lengths on specific chromosome arms with different approach – a method ATLAS (advanced telomere length analysis in *S. cerevisiae*). This method was primary used for analysis of telomeres in budding yeasts, which possess with very heterogeneous telomeres. Authors used tailing of genomic DNA with multiple cytosines by terminal transferase as the first step of the ATLAS protocol (Zubko et al., 2016). This approach can be used as solution for probable absence of G-overhangs in *pptr* mutants. The tailing reaction will be used as a pre-step of the PETRA method. To the C-tailed genomic DNA telomere primer containing multiple guanines will anneal. This primer will be extended and amplified by PCR.

The absence of telomere G-overhang is one of characteristics of cell lines with activated ALT mechanism. To verify the results of PETRA, direct analysis of G-overhangs in wild-type and *pptr* mutant lines was proceed by PENT reaction. The method is based on the annealing of the C-rich telomere primer on native genomic DNA and its extension with DNA polymerase possessing 5' → 3' exonuclease activity. Furthermore, the reaction mixture lacks dGTP, so the reaction stops at the first cytosine on the template strand. Nonetheless, the telomere-specific hybridization signals indicating the presence of telomere 3' G-overhang were present not only in wild-type samples but also in *pptr* mutants (**Figure 8.12**). The result is therefore in contradiction with observation of PETRA analysis. Moreover, the length of these telomere-specific signal was assessed to around 2.5 kb, which is in conflict with reported telomere length in *P. patens* which is about 1.5 kb.

In order to arrive at a conclusive result regarding the presence or absence of telomere G-overhangs in *pptr* mutants, further tests are planned. In the first place, the specificity of primer annealing will be tested by treatment of wild-type samples by exonuclease I to digest the 3' G-overhang. Furthermore, the PENT reaction will be performed with PETRA-T primer from the analysis of telomere length on specific chromosome arm.

Beside changes in telomere length and telomere chromatin structure, presence of extrachromosomal circles extruded from telomeres is other characteristics tightly connected with the ALT mechanism. In Zellinger et al. (2007), it was shown that *A. thaliana ku70* mutant with telomeres elongated by telomerase-independent ALT mechanism has elevated level of t-circles, supporting the extrachromosomal circles as a strong biomarker of ALT cells. DNA

isolated from *ku70* mutant was used as positive control in analysis of level of t-circles in *pptr* mutants. However, results from the pilot experiment (**Figure 8.14**) showed lower levels of t-circles in *pptr* mutants as well as in this positive control. Despite t-circles, which are composed of double-stranded telomere DNA, C- and G-circle – single stranded extrachromosomal telomere circles containing C- and G- strand of ancestral t-circle, respectively – can be present in cell lines with activated ALT mechanism. From those, C-circles were presented as the most abundant extrachromosomal telomere circles in cell lines with telomeres elongated by ALT (Henson et al., 2009).

Therefore, the primer used in rolling circle amplification step was change. In case of t-circle analysis, ThioTel primer with $(CCCTAAA)_3$ sequence with thiophosphate linkages between three 3' terminal nucleotides was used (Zellinger et al., 2007). To detect C-circles, PlTelG primer with $(GGGATTT)_4$ sequence was used in the first step of the reaction. Significantly elevated level of C-circles was detected in *pptr* mutants (**Figure 8.15**), which seems promising. However, similarly as in analysis of t-circles, level of C-circles in *ku70* mutant was the same as in *A. thaliana* sild-type samples, which significantly compromises reliability of all results. Thus, further investigation of extrachromosomal telomere circles in *pptr* mutants will be conducted in the future.

Preliminary analysis of Nanopore sequencing data revealed spread of subtelomere sequence across the whole genome especially into telomeres in *pptr* mutants. Dot blot analysis confirmed an elevated level of ISiT in *pptr* mutants compared to wild-type (**Figure 8.13**). This is consistent with the restructuring of the telomere chromatin due to the loss of the TR gene and ALT activation in the mutant line.

Since the *pptr* mutants are knock-out mutants which totally lack gene for TR, telomerase is inactivated in these plants, as showed in Fajkus et al. (2021). Nevertheless, *in vitro* analysis of telomerase activity by TRAP showed zero difference between wild-type and *pptr* mutant samples (**Figure 8.17**). This is not the first unsuccessful attempt to analyse telomerase activity in *P. patens*. We are regularly experiencing problems with *P. patens* telomerase activity assessments in our research group despite enormous optimizations (e. g., unpublished data from doc. Mgr. Miloslava Fojtová, CSc.; Mgr. Anna Rudolfová; Mgr. Lucie Bozděchová, Ph.D.). That's why I decided to try out so many different primer combinations. Although the initial results looked promising, as in previous experiments it was usually difficult to detect any signal in the wild-type samples, patterns in wild-type and *pptr* samples were fully comparable. Since we are sure,

that the TR gene is not active in *pptr* line and, consequently, telomerase cannot be active without its TR subunit, this is almost certainly a technical issue.

To study the dynamics of modulation of telomere length and structure of telomere chromatin during switch of telomere maintenance from telomerase-dependent to ALT mechanism we plan to analyse early stages after *de novo* construction of *pptr* mutants. For this purpose, amplification of 35S:HygR cassette, which will serve as an insert for *P. patens* transformation was successfully performed. However, subsequent transformation of protoplasts derived from wild-type 7-day-cultivated protonema of *P. patens* was repeatedly unsuccessful due to several contaminations (**Figure 8.2**). If the occurrence of contamination after transformation and subsequent cultivation on mannitol-rich medium continuous even in the future, different approach for protonema homogenization will be tested – instead of using blender homogenizer, sterile beads and homogenization shaker will be used.

10 Conclusion

Telomeres are nucleoprotein structures localized at the ends of linear eukaryotic chromosomes securing the solution for end-protection and end-replication problems. The end-replication problem is connected with constitutive shortening of telomeres every cell cycle. Length of telomeres is maintained by nucleoprotein enzyme telomerase or by telomerase-independent mechanism, ALT.

In this diploma thesis, the consequences of the ALT activation in *P. patens* mutants with the loss of telomerase RNA were studied. Analysis of bulk telomere length confirmed rapid changes reflected in shortened telomeres and stronger telomere specific signal, and indicates probable changes in the structure of telomere chromatin. However, analysis of the chromatin structure *via* MNase digestion revealed no strong distinction between wild-type and mutant samples. It is planned to apply other approaches for the telomere chromatin study.

The telomere length on specific chromosome arms could not be detected due to signal absence in *pptr* mutant samples. These data indicated probable loss of the telomere 3' G-overhang. This hypothesis was tested with an alternative approach. Its result showed no difference between wild-type and *pptr* mutant. Nonetheless, the length of telomere-specific hybridization signal has different length than telomeres of *P. patens* in TRF analysis. Therefore, analysis of G-overhangs will be repeated in future research.

It was also confirmed that in *pptr* mutant with activated ALT was elevated abundance of a specific subtelomere sequence, which was spread across a whole genome and especially into telomeres. This is consistent with the modulated structure of the telomere chromatin.

Level of extrachromosomal telomere circles – one of the characteristics of ALT cell lines – was slightly higher in *pptr* mutant compared to wild-type. Also here other optimisations are planned, because the analyses of the positive controls were not consistent with previously obtained data.

The vectors for *P. patens* protoplasts transformation to create new *pptr* mutant for the detailed study of telomere dynamics during the switch from telomerase-dependent to telomerase-independent telomere maintenance was successfully amplified. The transformation was unsuccessful due to culture contamination. The protoplast transformation will be repeated in the future research.

Results obtained during this diploma research contributed to a solution of a project elucidating the mechanisms enabling the long-term stability of chromosomes in plants with an inactive telomerase. In the further research, it is planned to restore telomerase activity in *pptr* mutants and analyse the telomere dynamics.

Furthermore, RNAseq data generated from the stable *pptr* mutant will be analysed. These data will be used to identify respective changes in levels of HR-related genes transcripts, again, to get closer insight into details of switching from telomerase-dependent to telomerase-independent mechanism of telomere maintenance.

Bibliography

ADAMUSOVÁ K., KHOSRAVI S., FUJIMOTO S., HOUBEN A., MATSUNAGA S., FAJKUS J., FOJTOVÁ M. 2020. Two Combinatorial Patterns of Telomere Histone Marks in Plants with Canonical and Non-canonical Telomere Repeats. *Plant J.* 102(4): 678–687. doi: 10.1111/tpj.14653

ANGELIS K.J., ZÁVESKÁ DRÁBKOVÁ L., VÁGNEROVÁ R., HOLÁ M. 2023. RAD51 and RAD51B Play Diverse Roles in the Repair of DNA Double Strand Breaks in Physcomitrium patens. *Genes.* 14(2): 305. doi: 10.3390/genes14020305

ANTAL M., BOROS É., SOLYMOSY F., KISS T. 2002. Analysis of the Structure of Human Telomerase RNA in Vivo. *Nucleic Acids Res.* 30(4): 912–920. doi: 10.1093/nar/30.4.912

ARIF M.A., HISS M., TOMEK M., BUSCH H., MEYBERG R., TINTELNOT S., RESKI R., RENSING S.A., FRANK W. 2019. ABA-Induced Vegetative Diaspore Formation in Physcomitrella patens. *Front. Plant Sci.* 10: 315. doi: 10.3389/fpls.2019.00315

AUTEXIER C., LUE N.F. 2006. The Structure and Function of Telomerase Reverse Transcriptase. *Annu. Rev. Biochem.* 75: 493–517. doi: 10.1146/annurev.biochem.75.103004.142412

BEIKE A.K., VON STACKELBERG M., SCHALLENBERG-RÜDINGER M., HANKE S.T., FOLLO M., QUANDT D., MCDANIEL S.F., RESKI R., TAN B.C., RENSING S.A. 2014. Molecular Evidence for Convergent Evolution and Allopolyploid Speciation within the Physcomitrium-Physcomitrella Species Complex. *BMC Evol. Biol.* 14: 158. doi: 10.1186/1471-2148-14-158

BILAUD T., KOERING C.E., BINET-BRASSELET E., ANCELIN K., POLLICE A., GASSER S.M., GILSON E. 1996. The Telobox, a Myb-Related Telomeric DNA Binding Motif Found in Proteins from Yeast, Plants and Human. *Nucleic Acids Res.* 24(7): 1294–1303. doi: 10.1093/nar/24.7.1294

BOX J.A., BUNCH J.T., ZAPPULLA D.C., GLYNN E.F., BAUMANN P. 2008. A Flexible Template Boundary Element in the RNA Subunit of Fission Yeast Telomerase. *J. Biol. Chem.* 283(35): 24224–24233. doi: 10.1074/jbc.M802043200

BOZDĚCHOVÁ L., HAVLOVÁ K., FAJKUS P., FAJKUS J. 2024. Analysis of Telomerase RNA Structure in *Physcomitrium patens* Indicates Functionally Relevant Transitions Between OPEN and CLOSED Conformations. *J. Mol. Biol.* 436(4): 168417. doi: 10.1016/j.jmb.2023.168417

BROCCOLI D., SMOGORZEWSKA A., CHONG L., DE LANGE T. 1997. Human Telomeres Contain Two Distinct Myb-Related Proteins, TRF1 and TRF2. *Nat. Genet.* 17(2): 231–235. doi: 10.1038/ng1097-231

BRYAN T.M., ENGLEZOU A., GUPTA J., BACCHETTI S., REDDEL R.R. 1995. Telomere Elongation in Immortal Human Cells without Detectable Telomerase Activity. *EMBO J.* 14(17): 4240–4248. doi: 10.1002/j.1460-2075.1995.tb00098.x

BURKI F., ROGER A.J., BROWN M.W., SIMPSON A.G.B. 2020. The New Tree of Eukaryotes. *Trends Ecol. Evol*. 35(1): 43–55. doi: 10.1016/j.tree.2019.08.008

CASACUBERTA E. 2017. Drosophila: Retrotransposons Making up Telomeres. *Viruses.* 9(7): 192. doi: 10.3390/v9070192

CESARE A.J., REDDEL R.R. 2010. Alternative Lengthening of Telomeres: Models, Mechanisms and Implications. *Nat. Rev. Genet*. 11(5): 319–330. doi: 10.1038/nrg2763

CHOI W.S., WENG P.J., YANG W. 2022. Flexibility of Telomerase in Binding the RNA Template and DNA Telomeric Repeat. *Proc. Natl. Acad. Sci. U. S. A*. 119(1): e2116159118. doi: 10.1073/pnas.2116159118

CHUNG J., KHADKA P., CHUNG I.K. 2012. Nuclear Import of hTERT Requires a Bipartite Nuclear Localization Signal and Akt-Mediated Phosphorylation. *J. Cell Sci*. 125: 2684–2697. doi: 10.1242/jcs.099267

COLE D.I., LEGASSIE J.D., BONIFACIO L.N., SEKARAN V.G., DING F., DOKHOLYAN N.V., JARSTFER M.B. 2012. New Models of Tetrahymena Telomerase RNA from Experimentally Derived Constraints and Modeling. *J. Am. Chem. Soc*. 134(49): 20070–20080. doi: 10.1021/ja305636u

CONOMOS D., PICKETT H., REDDEL R. 2013. Alternative Lengthening of Telomeres: Remodelling the Telomere Architecture. *Front. Oncol*. 3: 27. doi: 10.3389/fonc.2013.00027

CONOMOS D., STUTZ M.D., HILLS M., NEUMANN A.A., BRYAN T.M., REDDEL R.R., PICKETT H.A. 2012. Variant Repeats Are Interspersed Throughout the Telomeres and Recruit Nuclear Receptors in ALT Cells. *J. Cell Biol*. 199(6): 893–906.doi: 10.1083/jcb.201207189

COUDERT Y., PALUBICKI W., LJUNG K., NOVAK O., LEYSER O., HARRISON C.J. 2015. Three Ancient Hormonal Cues Co-Ordinate Shoot Branching in a Moss. *eLife*. 4: e06808. doi: 10.7554/eLife.06808

COVE D. 2005. The Moss Physcomitrella patens. *Annu. Rev. Genet*. 39: 339–358. doi: 10.1146/annurev.genet.39.073003.110214

COVE D.J., KNIGHT C.D. 1993. The Moss Physcomitrella patens, a Model System with Potential for the Study of Plant Reproduction. *Plant Cell*. 5(10): 1483–1488. doi: 10.1105/tpc.5.10.1483

COVE D.J., PERROUD P.-F., CHARRON A.J., MCDANIEL S.F., KHANDELWAL A., QUATRANO R.S. 2009. The Moss Physcomitrella patens: a Novel Model System for Plant Development and Genomic Studies. *Cold Spring Harb. Protoc*. 2009(2): pdb.emo115. doi: 10.1101/pdb.emo115

DÉJARDIN J., KINGSTON R.E. 2009. Purification of Proteins Associated with Specific Genomic Loci. *Cell*. 136(1): 175–186. doi: 10.1016/j.cell.2008.11.045

EGAN E.D., COLLINS K. 2012. Biogenesis of Telomerase Ribonucleoproteins. *RNA*. 18(10): 1747–1759. doi: 10.1261/rna.034629.112

FAJKUS J., FULNEČKOVÁ J., HULÁNOVÁ M., BERKOVÁ K., ŘÍHA K., MATYÁŠEK R. 1998. Plant Cells Express Telomerase Activity upon Transfer to Callus Culture, without Extensively Changing Telomere Lengths. *Mol. Gen. Genet. MGG.* 260(5): 470–474. doi: 10.1007/s004380050918

FAJKUS, J., KOVAŘÍK, A., KRÁLOVICS, R., 1996. Telomerase Activity in Plant Cells. *FEBS Lett.* 391(3): 307–309. doi: 10.1016/0014-5793(96)00757-0

FAJKUS P., KILAR A., NELSON A.D.L., HOLÁ M., PEŠKA V., GOFFOVÁ I., FOJTOVÁ M., ZACHOVÁ D., FULNEČKOVÁ J., FAJKUS J. 2021. Evolution of Plant Telomerase RNAs: Farther to the Past, Deeper to the Roots. *Nucleic Acids Res*. 49(13): 7680–7694. doi: 10.1093/nar/gkab545

FAJKUS P., PEŠKA V., SITOVÁ Z., FULNEČKOVÁ J., DVOŘÁČKOVÁ M., GOGELA R., SÝKOROVÁ E., HAPALA J., FAJKUS J. 2016. Allium Telomeres Unmasked: the Unusual Telomeric Sequence (CTCGGTTATGGG)n Is Synthesized by Telomerase. *Plant J*. 85(3): 337–347. doi: 10.1111/tpj.13115

FAJKUS P., PEŠKA V., ZÁVODNÍK M., FOJTOVÁ M., FULNEČKOVÁ J., DOBIAS Š., KILAR A., DVOŘÁČKOVÁ M., ZACHOVÁ D., NEČASOVÁ I., SIMS J., SÝKOROVÁ E., FAJKUS J. 2019. Telomerase RNAs in Land Plants. *Nucleic Acids Res*. 47(18): 9842–9856. doi: 10.1093/nar/gkz695

FENG X., HSU S.-J., BHATTACHARJEE A., WANG Y., DIAO J., PRICE C.M. 2018. CTC1-STN1 Terminates Telomerase while STN1-TEN1 Enables C-strand Synthesis during Telomere Replication in Colon Cancer Cells. *Nat. Commun*. 9: 2827. doi: 10.1038/s41467-018-05154-z

FITZGERALD M.S., MCKNIGHT T.D., SHIPPEN D.E. 1996. Characterization and Developmental Patterns of Telomerase Expression in Plants. *Proc. Natl. Acad. Sci*. 93(25): 14422–14427. doi: 10.1073/pnas.93.25.14422

FOJTOVÁ M., FAJKUS P., POLANSKÁ P., FAJKUS J. 2015a. Terminal Restriction Fragments (TRF) Method to Analyze Telomere Lengths. *Bio-Protoc*. 5(23). doi: 10.21769/BioProtoc.1671

FOJTOVÁ M., SÝKOROVÁ E., NAJDEKROVÁ L., POLANSKÁ P., ZACHOVÁ D., VAGNEROVÁ R., ANGELIS K.J., FAJKUS J. 2015b. Telomere Dynamics in the Lower Plant Physcomitrella patens. *Plant Mol. Biol*. 87(6): 591–601. doi: 0.1007/s11103-015-0299-9

FUJIWARA H., OSANAI M., MATSUMOTO T., KOJIMA K.K. 2005. Telomere-Specific Non-LTR Retrotransposons and Telomere Maintenance in the Silkworm, Bombyx mori. *Chromosome Res*. 13(5): 455–467. doi: 10.1007/s10577-005-0990-9

FULCHER N., RIHA K. 2016. Using Centromere Mediated Genome Elimination to Elucidate the Functional Redundancy of Candidate Telomere Binding Proteins in Arabidopsis thaliana. *Front. Genet*. 6: 349. doi: 10.3389/fgene.2015.00349

GOFFOVÁ I., VÁGNEROVÁ R., PEŠKA V., FRANEK M., HAVLOVÁ K., HOLÁ M., ZACHOVÁ D., FOJTOVÁ M., CUMING A., KAMISUGI Y., ANGELIS K.J., FAJKUS J. 2019. Roles of RAD51 and RTEL1 in Telomere and rDNA Stability in Physcomitrella patens. *Plant J.* 98(6): 1090–1105. doi: 10.1111/tpj.14304

GRIFFITH J.D., COMEAU L., ROSENFIELD S., STANSEL R.M., BIANCHI A., MOSS H., DE LANGE T. 1999. Mammalian Telomeres End in a Large Duplex Loop. *Cell*. 97(4): 503–514. doi: 10.1016/S0092-8674(00)80760-6

HEACOCK M., SPANGLER E., RIHA K., PUIZINA J., SHIPPEN D.E. 2004. Molecular Analysis of Telomere Fusions in Arabidopsis: Multiple Pathways for Chromosome End-Joining. *EMBO J*. 23(11): 2304–2313. doi: 10.1038/sj.emboj.7600236

HENSON J.D., CAO Y., HUSCHTSCHA L.I., CHANG A.C., AU A.Y.M., PICKETT H.A., REDDEL R.R. 2009. DNA C-circles Are Specific and Quantifiable Markers of Alternative-Lengthening-of-Telomeres Activity. *Nat. Biotechnol*. 27(12): 1181–1185. doi: 10.1038/nbt.1587

HISS M., MEYBERG R., WESTERMANN J., HAAS F.B., SCHNEIDER L., SCHALLENBERG-RÜDINGER M., ULLRICH K.K., RENSING S.A. 2017. Sexual Reproduction, Sporophyte Development and Molecular Variation in the Model Moss Physcomitrella patens: Introducing the Ecotype Reute. *Plant J*. 90(3): 606–620. doi: 10.1111/tpj.13501

HU J., HWANG S.S., LIESA M., GAN B., SAHIN E., JASKELIOFF M., DING Z., YING H., BOUTIN A.T., ZHANG H., JOHNSON S., IVANOVA E., KOST-ALIMOVA M., PROTOPOPOV A., WANG Y.A., SHIRIHAI O.S., CHIN L., DEPINHO R.A. 2012. Anti-Telomerase Therapy Provokes ALT and Mitochondrial Adaptive Mechanisms in Cancer. *Cell*. 148(4): 651–663. doi: 10.1016/j.cell.2011.12.028

IJDO J.W., WELLS R.A., BALDINI A., REEDERS S.T. 1991. Improved Telomere Detection Using a Telomere Repeat Probe (TTAGGG)n Generated by PCR. *Nucleic Acids Res*. 19(17): 4780. doi: 10.1093/nar/19.17.4780

JANOUŠKOVÁ E., NEČASOVÁ I., PAVLOUŠKOVÁ J., ZIMMERMANN M., HLUCHÝ M., MARINI V., NOVÁKOVÁ M., HOFR C. 2015. Human Rap1 Modulates TRF2 Attraction to Telomeric DNA. *Nucleic Acids Res*. 43(5): 2691–2700. doi: 10.1093/nar/gkv097

JANOVIČ T., PEREZ G.I., BOELTING G., SCHMIDT J.C. 2025. TRF1 and TRF2 Form Distinct Shelterin Subcomplexes at Telomeres. *Cell Rep*. 44(9): 116178. doi: 10.1016/j.celrep.2025.116178

KAMISUGI Y., SCHLINK K., RENSING S.A., SCHWEEN G., VON STACKELBERG M., CUMING A.C., RESKI R., COVE D.J. 2006. The Mechanism of Gene Targeting in Physcomitrella patens: Homologous Recombination, Concatenation and Multiple Integration. *Nucleic Acids Res*. 34(21): 6205–6214. doi: 10.1093/nar/gkl832

KOBAYASHI C.R., CASTILLO-GONZÁLEZ C., SURVOTSEVA Y., CANAL E., NELSON A.D.L., SHIPPEN D.E. 2019. Recent Emergence and Extinction of the Protection of Telomeres 1c Gene in Arabidopsis thaliana. *Plant Cell Rep*. 38(9): 1081–1097. doi: 10.1007/s00299-019-02427-9

KUCHAŘ M., FAJKUS J. 2004. Interactions of Putative Telomere-Binding Proteins in Arabidopsis thaliana: Identification of Functional TRF2 Homolog in Plants. *FEBS Lett*. 578(3): 311–315. doi: 10.1016/j.febslet.2004.11.021

KUSOVÁ A., HOLÁ M., PETROVÁ I.G., RUDOLF J., ZACHOVÁ D., SKALÁK J., HEJÁTKO J., KLODOVÁ B., PŘEROVSKÁ T., LYČKA M., SÝKOROVÁ E., BERTRAND Y.J.K., FAJKUS J., HONYS D., SCHRUMPFOVÁ P.P. 2025. TRB Proteins in Moss Reveal Their Evolutionarily Conserved Roles in Plant Development and Telomere Maintenance. *Plant J*. 124(3): e70574. doi: 10.1111/tpj.70574

KUSOVÁ A., STEINBACHOVÁ L., PŘEROVSKÁ T., DRÁBKOVÁ L.Z., PALEČEK J., KHAN A., RIGÓOVÁ G., GADIOU Z., JOURDAIN C., STRICKER T., SCHUBERT D., HONYS D., SCHRUMPFOVÁ P.P. 2023. Completing the TRB Family: Newly Characterized Members Show Ancient Evolutionary Origins and Distinct Localization, Yet Similar Interactions. *Plant Mol. Biol*. 112(1–2): 61–83. doi: 10.1007/s11103-023-01348-2

LANG D., ULLRICH K.K., MURAT F., FUCHS J., JENKINS J., HAAS F.B., PIEDNOEL M., GUNDLACH H., VAN BEL M., MEYBERG R., VIVES C., MORATA J., SYMEONIDI A., HISS M., MUCHERO W., KAMISUGI Y., SALEH O., BLANC G., DECKER E.L., VAN GESSEL N. GRIMWOOD J., HAYES R.D., GRAHAM S.W., GUNTER L.E., MCDANIEL S.F., HOERNSTEIN S.N.W., LARSSON A., LI F.-W., PERROUD P.-F., PHILLIPS J., RANJAN P., ROKSHAR D.S., ROTHFELS C.J., SCHNEIDER L., SHU S., STEVENSON D.W., THÜMMLER F., TILLICH M., VILLARREAL AGUILAR J.C., WIDIEZ T., WONG G.K.-S., WYMORE A., ZHANG Y., ZIMMER A.D., QUATRANO R.S., MAYER K.F.X., GOODSTEIN D., CASACUBERTA J.M., VANDEPOELE K., RESKI R., CUMING A.C., TUSKAN G.A., MAUMUS F., SALSE J., SCHMUTZ J., RENSING S.A. 2018. The Physcomitrella patens Chromosome-Scale Assembly Reveals Moss Genome Structure and Evolution. *Plant J*. 93(3): 515–533. doi: 10.1111/tpj.13801

LANGE T. DE 2005. Shelterin: The Protein Complex That Shapes and Safeguards Human Telomeres. *Genes Dev*. 19(18): 2100–2110. doi: 10.1101/gad.1346005

LATRICK C.M., CECH T.R. 2010. POT1–TPP1 Enhances Telomerase Processivity by Slowing Primer Dissociation and Aiding Translocation. *EMBO J*. 29(5): 924–933. doi: 10.1038/emboj.2009.409

LEE M., HILLS M., CONOMOS D., STUTZ M.D., DAGG R.A., LAU L.M.S., REDDEL R.R., PICKETT H.A. 2014. Telomere Extension by Telomerase and ALT Generates Variant Repeats by Mechanistically Distinct Processes. *Nucleic Acids Res*. 42(3): 1733–1746. doi: 10.1093/nar/gkt1117

LEI M., PODELL E.R. CECH T.R. 2004. Structure of Human POT1 Bound to Telomeric Single-Stranded DNA Provides a Model for Chromosome End-Protection. *Nat. Struct. Mol. Biol*. 11(12): 1223–1229. doi: 10.1038/nsmb867

LIM C.J., CECH T.R. 2021. Shaping Human Telomeres: From Shelterin and CST Complexes to Telomeric Chromatin Organization. *Nat. Rev. Mol. Cell Biol*. 22: 283–298. doi: 10.1038/s41580-021-00328-y

LINGNER J., HUGHES T.R., SHEVCHENKO A., MANN M., LUNDBLAD V., CECH T.R. 1997. Reverse Transcriptase Motifs in the Catalytic Subunit of Telomerase. *Science*. 276(5312): 561–567. doi: 10.1126/science.276.5312.561

LIU Y.-C., VIDALI L. 2011. Efficient Polyethylene Glycol (PEG) Mediated Transformation of the Moss Physcomitrella patens. *J. Vis. Exp.* 19(50): 2560. doi: 10.3791/2560

LONDOÑO-VALLEJO J.A., DER-SARKISSIAN H., CAZES L., BACCHETTI S., REDDEL R.R. 2004. Alternative Lengthening of Telomeres Is Characterized by High Rates of Telomeric Exchange. *Cancer Res*. 64(7): 2324–2327. doi: 10.1158/0008-5472.CAN-03-4035

LYČKA M., PESKA V., DEMKO M., SPYROGLOU I., KILAR A., FAJKUS J., FOJTOVÁ M. 2021. WALTER: An Easy Way to Online Evaluate Telomere Lengths from Terminal Restriction Fragment Analysis. *BMC Bioinformatics*. 22(1): 145. doi: 10.1186/s12859-021-04064-0

MANSISIDOR A.R., RISCA V.I. 2022. Chromatin Accessibility: Methods, Mechanisms, and Biological Insights. *Nucleus*. 13(1): 236–276. doi: 10.1080/19491034.2022.2143106

MARIAN C.O., BORDOLI S.J., GOLTZ M., SANTARELLA R.A., JACKSON L.P., DANILEVSKAYA O., BECKSTETTE M., MEELEY R., BASS H.W. 2003. The Maize Single myb histone 1 Gene, Smh1, Belongs to a Novel Gene Family and Encodes a Protein That Binds Telomere DNA Repeats in Vitro. *Plant Physiol*. 133(3): 1336–1350. doi: 10.1104/pp.103.026856

MARZEC P., ARMENISE C., PÉROT G., ROUMELIOTI F.-M., BASYUK E., GAGOS S., CHIBON F., DÉJARDIN J. 2015. Nuclear-Receptor-Mediated Telomere Insertion Leads to Genome Instability in ALT Cancers. *Cell*. 160(5): 913–927. doi: 10.1016/j.cell.2015.01.044

MCCLINTOCK B. 1942. The Fusion of Broken Ends of Chromosomes Following Nuclear Fusion. *Proc. Natl. Acad. Sci. U. S. A*. 28(11): 458–463. doi: 10.1073/pnas.28.11.458

MCCLINTOCK B. 1938. The Fusion of Broken Ends of Sister Half-Chromatids Following Chromatid Breakage at Meiotic Anaphases. *Res. Bull. Mo. agric. Exp. Sia*. 290: 1–48.

MEDINA R., JOHNSON M., LIU Y., WILDING N., HEDDERSON T.A., WICKETT N., GOFFINET B. 2018. Evolutionary Dynamism in Bryophytes: Phylogenomic Inferences Confirm Rapid Radiation in the Moss Family Funariaceae. *Mol. Phylogenet. Evol*. 120: 240–247. doi: 10.1016/j.ympev.2017.12.002

MEDINA R., JOHNSON M.G., LIU Y., WICKETT N.J., SHAW A.J., GOFFINET B. 2019. Phylogenomic Delineation of Physcomitrium (Bryophyta: Funariaceae) Based on Targeted Sequencing of Nuclear Exons and Their Flanking Regions Rejects the Retention of Physcomitrella, Physcomitridium and Aphanorrhegma. *J. Syst. Evol*. 57(4): 404–417. doi: 10.1111/jse.12516

MEIER B., CLEJAN I., LIU Y., LOWDEN M., GARTNER A., HODGKIN J., AHMED S. 2006. trt-1 Is the Caenorhabditis elegans Catalytic Subunit of Telomerase. *PLoS Genet*. 2(2): e18. doi: 10.1371/journal.pgen.0020018

MENAND B., CALDER G., DOLAN L. 2007. Both Chloronemal and Caulonemal Cells Expand by Tip Growth in the Moss Physcomitrella patens. *J. Exp. Bot*. 58(7): 1843–1849. doi: 10.1093/jxb/erm047

MÜLLER H.J. 1938. The Remaking of Chromosomes. *Collecting Net*. 13: 181–198.

NAKAMURA T.M., MORIN G.B., CHAPMAN K.B., WEINRICH S.L., ANDREWS W.H., LINGNER J., HARLEY C.B., CECH T.R. 1997. Telomerase Catalytic Subunit Homologs from Fission Yeast and Human. *Science.* 277(5328): 955–959. doi: 10.1126/science.277.5328.955

NIEDERER R.O., ZAPPULLA D.C. 2015. Refined Secondary-Structure Models of the Core of Yeast and Human Telomerase RNAs Directed by SHAPE. *RNA*. 21(2): 254–261. doi: 10.1261/rna.048959.114

OLOVNIKOV A.M. 1971. Principle of Marginotomy in Template Synthesis of Polynucleotides. *Dokl. Akad. Nauk SSSR*. 201(6): 1496–1499.

O'SULLIVAN R.J., GREENBERG R.A. 2025. Mechanisms of Alternative Lengthening of Telomeres. *Cold Spring Harb. Perspect. Biol*. 17(1): a041690. doi: /10.1101/cshperspect.a041690

PEŠKA V., FAJKUS P., FOJTOVÁ M., DVOŘÁČKOVÁ M., HAPALA J., DVOŘÁČEK V., POLANSKÁ P., LEITCH A.R., SÝKOROVÁ E., FAJKUS J. 2015. Characterisation of an Unusual Telomere Motif (TTTTTTAGGG)n in the Plant Cestrum elegans (Solanaceae), a Species with a Large Genome. *Plant J*. 82(4): 644–654. doi: 10.1111/tpj.12839

PESKA V., GARCIA S. 2020. Origin, Diversity, and Evolution of Telomere Sequences in Plants. *Front. Plant Sci*. 11: 117. doi: 10.3389/fpls.2020.00117

PEŠKA V., SCHRUMPFOVÁ P.P., FAJKUS J. 2011. Using the Telobox to Search for Plant Telomere Binding Proteins. *Curr. Protein Pept. Sci*. 12(2): 75–83. doi: 10.2174/138920311795684968

PODLEVSKY J.D., CHEN J.J.-L. 2016. Evolutionary Perspectives of Telomerase RNA Structure and Function. *RNA Biol*. 13(8): 720–732. doi: 10.1080/15476286.2016.1205768

PROCHÁZKOVÁ SCHRUMPFOVÁ P., FOJTOVÁ M., FAJKUS J. 2019. Telomeres in Plants and Humans: Not So Different, Not So Similar. *Cells*. 8(1): 58. doi: 10.3390/cells8010058

PROCHÁZKOVÁ SCHRUMPFOVÁ P., VYCHODILOVÁ I., DVOŘÁČKOVÁ M., MAJERSKÁ J., DOKLÁDAL L., SCHOŘOVÁ Š., FAJKUS J. 2014. Telomere Repeat Binding Proteins Are Functional Components of Arabidopsis Telomeres and Interact with Telomerase. *Plant J.* 77(5): 770–781. doi: 10.1111/tpj.12428

RENSING S.A., GOFFINET B., MEYBERG R., WU S.-Z., BEZANILLA M. 2020. The Moss Physcomitrium (Physcomitrella) patens: A Model Organism for Non-Seed Plants. *Plant Cell*. 32(5): 1361–1376. doi: 10.1105/tpc.19.00828

RENSING S.A., LANG D., ZIMMER A.D., TERRY A., SALAMOV A., SHAPIRO H., NISHIYAMA T., PERROUD P.-F., LINDQUIST E.A., KAMISUGI Y., TANAHASHI T., SAKAKIBARA K., FUJITA T., OISHI K., SHIN-I T., KUROKI Y., TOYODA A., SUZUKI Y., HASHIMOTO S., YAMAGUCHI K., SUGANO S., KOHARA Y., FUJIYAMA A., ANTEROLA A., AOKI S., ASHTON N., BARBAZUK W.B., BARKER E., BENNETZEN J.L., BLANKENSHIP R., CHO S.H., DUTCHER S.K., ESTELLE M., FAWCETT J.A., GUNDLACH H., HANADA K., HEYL A., HICKS K.A., HUGHES J., LOHR M., MAYER K., MELKOZERNOV A., MURATA T., NELSON D.R., PILS B., PRIGGE M., REISS B., RENNER T., ROMBAUTS S., RUSHTON P.J., SANDERFOOT A., SCHWEEN G., SHIU S.-H., STUEBER K., THEODOULOU F.L., TU H., VAN DE PEER Y., VERRIER P.J., WATERS E., WOOD A., YANG L., COVE D., CUMING A.C., HASEBE M., LUCAS S., MISHLER B.D., RESKI R., GRIGORIEV I.V., QUATRANO R.S., BOORE J.L. 2008. The Physcomitrella Genome Reveals Evolutionary Insights into the Conquest of Land by Plants. *Science*. 319(5859): 64–69. doi: 10.1126/science.1150646

RHODES D., LIPPS H.J. 2015. G-Quadruplexes and Their Regulatory Roles in Biology. *Nucleic Acids Res*. 43(18): 8627–8637. doi: 10.1093/nar/gkv862

RICHARDS E.J., AUSUBEL F.M. 1988. Isolation of a Higher Eukaryotic Telomere from Arabidopsis thaliana. *Cell*. 53(1): 127–136. doi: 10.1016/0092-8674(88)90494-1

RIHA K., FAJKUS J., SIROKY J., VYSKOT B. 1998. Developmental Control of Telomere Lengths and Telomerase Activity in Plants. *Plant Cell*. 10(10): 1691–1698. doi: 10.1105/tpc.10.10.1691

RIHA K., MCKNIGHT T.D., FAJKUS J., VYSKOT B., SHIPPEN D.E. 2000. Analysis of the G-Overhang Structures on Plant Telomeres: Evidence for Two Distinct Telomere Architectures. *Plant J.* 23(5): 633–641. doi: 10.1046/j.1365-313x.2000.00831.x

RŮČKOVÁ E., FRIML J., PROCHÁZKOVÁ SCHRUMPFOVÁ P., FAJKUS J. 2008. Role of Alternative Telomere Lengthening Unmasked in Telomerase Knock-Out Mutant Plants. *Plant Mol. Biol*. 66(6): 637–646. doi: 10.1007/s11103-008-9295-7

SASAKI T., FUJIWARA H. 2000. Detection and Distribution Patterns of Telomerase Activity in Insects. *Eur. J. Biochem*. 267(10): 3025–3031. doi: 10.1046/j.1432-1033.2000.01323.x

SCHAEFER D.G. 2002. A New Moss Genetics: Targeted Mutagenesis in Physcomitrella patens. *Annu. Rev. Plant Biol*. 53, 477–501. doi: 10.1146/annurev.arplant.53.100301.135202

SCHAEFER D.G., ZRŸD J.-P. 1997. Efficient Gene Targeting in the Moss Physcomitrella patens. *Plant J*. 11(6): 1195–1206. doi: 10.1046/j.1365-313X.1997.11061195.x

SCHMIDT J.C., CECH T.R. 2015. Human Telomerase: Biogenesis, Trafficking, Recruitment, and Activation. *Genes Dev*. 29(11): 1095–1105. doi: 10.1101/gad.263863.115

SCHRUMPFOVÁ P.P., FAJKUS J. 2020. Composition and Function of Telomerase—A Polymerase Associated with the Origin of Eukaryotes. *Biomolecules*. 10(10): 1425. doi: 10.3390/biom10101425

SCHWARTZ U., NÉMETH A., DIERMEIER S., EXLER J.H., HANSCH S., MALDONADO R., HEIZINGER L., MERKL R., LÄNGST G. 2019. Characterizing the Nuclease Accessibility of DNA in Human Cells to Map Higher Order Structures of Chromatin. *Nucleic Acids Res*. 47(3): 1239–1254. doi: 10.1093/nar/gky1203

SCHWEEN G., HOHE A., KOPRIVOVA A., RESKI R. 2003. Effects of Nutrients, Cell Density and Culture Techniques on Protoplast Regeneration and Early Protonema Development in a Moss, Physcomitrella patens. *J. Plant Physiol*. 160(2): 209–212. doi: 10.1078/0176-1617-00855

SEN D., GILBERT W. 1988. Formation of Parallel Four-Stranded Complexes by Guanine-Rich Motifs in DNA and Its Implications for Meiosis. *Nature*. 334(6180): 364–366. doi: 10.1038/334364a0

SFEIR A., DE LANGE T. 2012. Removal of Shelterin Reveals the Telomere End-Protection Problem. *Science*. 336(6081): 593–597. doi: 10.1126/science.1218498

SFEIR A., KOSIYATRAKUL S.T., HOCKEMEYER D., MACRAE S.L., KARLSEDER J., SCHILDKRAUT C.L., DE LANGE T. 2009. Mammalian Telomeres Resemble Fragile Sites and Require TRF1 for Efficient Replication. *Cell*. 138(1): 90–103. doi: 10.1016/j.cell.2009.06.021

SHAY J.W., WRIGHT W.E. 2005. Senescence and Immortalization: Role of Telomeres and Telomerase. *Carcinogenesis*. 26(5): 867–874. doi: 10.1093/carcin/bgh296

SIKORSKAITE S., RAJAMÄKI M.-L., BANIULIS D., STANYS V., VALKONEN J.P. 2013. Protocol: Optimised Methodology for Isolation of Nuclei from Leaves of Species in the Solanaceae and Rosaceae Families. *Plant Methods*. 9: 31. doi: 10.1186/1746-4811-9-31

SIMONET T., ZARAGOSI L.-E., PHILIPPE C., LEBRIGAND K., SCHOUTEDEN C., AUGEREAU A., BAUWENS S., YE J., SANTAGOSTINO M., GIULOTTO E., MAGDINIER F., HORARD B., BARBRY P., WALDMANN R., GILSON E. 2011. The Human TTAGGG Repeat Factors 1 and 2 Bind to a Subset of Interstitial Telomeric Sequences and Satellite Repeats. *Cell Res*. 21(7): 1028–1038. doi: 10.1038/cr.2011.40

SONG J., LOGESWARAN D., CASTILLO-GONZÁLEZ C., LI Y., BOSE S., AKLILU B.B., MA Z., POLKHOVSKIY A., CHEN J.J.-L., SHIPPEN D.E. 2019. The Conserved Structure of Plant

Telomerase RNA Provides the Missing Link for an Evolutionary Pathway from Ciliates to Humans. Proc. *Natl. Acad. Sci. U. S. A.* 116(49): 24542–24550. doi: 10.1073/pnas.1915312116

SOVÁKOVÁ P.P., MAGDOLENOVÁ A., KONEČNÁ K., RÁJECKÁ V., FAJKUS J., FOJTOVÁ M. 2018. Telomere Elongation Upon Transfer to Callus Culture Reflects the Reprogramming of Telomere Stability Control in Arabidopsis. *Plant Mol. Biol.* 98(1–2): 81–99. doi: 10.1007/s11103-018-0765-2

STANSEL R.M., DE LANGE T., GRIFFITH J.D. 2001. T-loop Assembly in Vitro Involves Binding of TRF2 Near the 3′ Telomeric Overhang. *EMBO J.* 20(19): 5532–5540. doi: 10.1093/emboj/20.19.5532

SÝKOROVÁ E., FAJKUS J. 2009. Structure—Function Relationships in Telomerase Genes. *Biol. Cell.* 101(7): 375–406. doi: 10.1042/BC20080205

SÝKOROVÁ E., LEITCH A.R., FAJKUS J. 2006. Asparagales Telomerases which Synthesize the Human Type of Telomeres. *Plant Mol. Biol.* 60(5): 633–646. doi: 10.1007/s11103-005-5091-9

TAKAHASHI H., OKAZAKI S., FUJIWARA H. 1997. A New Family of Site-Specific Retrotransposons, SART1, Is Inserted into Telomeric Repeats of the Silkworm, Bombyx mori. *Nucleic Acids Res.* 25(8): 1578–1584. doi: 10.1093/nar/25.8.1578

TIMASHEV L.A., DE LANGE T. 2020. Characterization of T-Loop Formation by TRF2. *Nucleus.* 11(1): 164–177. doi: 10.1080/19491034.2020.1783782

TRAN T.D., CAO H.X., JOVTCHEV G., NEUMANN P., NOVÁK P., FOJTOVÁ M., VU G.T.H., MACAS J., FAJKUS J., SCHUBERT I., FUCHS J. 2015. Centromere and Telomere Sequence Alterations Reflect the Rapid Genome Evolution within the Carnivorous Plant Genus Genlisea. *Plant J.* 84(6): 1087–1099. doi: 10.1111/tpj.13058

VÍTKOVÁ M., KRÁL J., TRAUT W., ZRZAVÝ J., MAREC F. 2005. The Evolutionary Origin of Insect Telomeric Repeats, (TTAGG)n. *Chromosome Res.* 13(2): 145–156. doi: 10.1007/s10577-005-7721-0

WANG Q., LIU J., CHEN Z., ZHENG K., CHEN C., HAO Y., TAN Z. 2011. G-Quadruplex Formation at the 3′ End of Telomere DNA Inhibits Its Extension by Telomerase, Polymerase and Unwinding by Helicase. *Nucleic Acids Res.* 39(14): 6229–6237. doi: 10.1093/nar/gkr164

WEBB C.J., ZAKIAN V.A. 2016. Telomerase RNA Is More Than a DNA Template. *RNA Biol.* 13(8): 683–689. doi: 10.1080/15476286.2016.1191725

WELLINGER R.J., ZAKIAN V.A. 2012. Everything You Ever Wanted to Know About Saccharomyces cerevisiae Telomeres: Beginning to End. *Genetics.* 191(4): 1073–1105. doi: 10.1534/genetics.111.137851

WU R.A., UPTON H.E., VOGAN J.M., COLLINS K. 2017. Telomerase Mechanism of Telomere Synthesis. *Annu. Rev. Biochem.* 86: 439–460. doi: 10.1146/annurev-biochem-061516-045019

ZELLINGER B., AKIMCHEVA S., PUIZINA J., SCHIRATO M., RIHA K. 2007. Ku Suppresses Formation of Telomeric Circles and Alternative Telomere Lengthening in Arabidopsis. *Mol. Cell*. 27(1): 163–169. doi: 10.1016/j.molcel.2007.05.025

ZHONG F.L., BATISTA L.F.Z., FREUND A., PECH M.F., VENTEICHER A.S., ARTANDI S.E. 2012. TPP1 OB-Fold Domain Controls Telomere Maintenance by Recruiting Telomerase to Chromosome Ends. *Cell*. 150(3): 481–494. doi: 10.1016/j.cell.2012.07.012

ZIMMERMANN M., KIBE T., KABIR S., DE LANGE T. 2014. TRF1 Negotiates TTAGGG Repeat-Associated Replication Problems by Recruiting the BLM Helicase and the TPP1/POT1 Repressor of ATR Signaling. *Genes Dev*. 28(22): 2477–2491. doi: 10.1101/gad.251611.114

ZIMMERMANN M., LOTTERSBERGER F., BUONOMO S.B., SFEIR A., DE LANGE T. 2013. 53BP1 Regulates DSB Repair Using Rif1 to Control 5' End Resection. *Science*. 339(6120): 700–704. doi: 10.1126/science.1231573

ZUBKO E.I., SHACKLETON J.L., ZUBKO M.K. 2016. ATLAS: An Advanced PCR-Method for Routine Visualization of Telomere Length in Saccharomyces cerevisiae. *Int. J. Biol. Macromol*. 93: 1285–1294. doi: 10.1016/j.ijbiomac.2016.09.006

Appendix A In gel hybridization protocol

A.1 Sample and gel preparation

Digestion was performed with 15 000 ng of genomic DNA mixed with $\frac{1}{10}$ volume of 10× rCutSmart buffer, 1 µl of *MseI* and filled up with sterile water to 20 µl (if the concentration of DNA was too low, total reaction volume was 30 µl). Digestion was performed at 37 °C for 17 h. Other day, 1 µl of *MseI* was added and digestion continued at 37 °C for another 5 h. If needed, the sample volume was reduced to 20 µl by lyophilisation.

Digested samples were separated by an electrophoresis on 1% agarose gel in 1× TAE overnight at 0.9 $V \cdot cm^{-1}$, and the gel was dried using Gel Drier. Dried gel was hybridized with radioactively end-labelled telomere oligonucleotide PlTelC according to **section 7.2.11.1**.

A.2 Native DNA hybridization with a radioactively labelled telomere probe

Prehybridization

1. Dried gel was placed into a closable box and Denhardt's hybridization solution was poured onto it.
2. Prehybridization was performed for 1 h at 55 °C in a hybridization oven.

Hybridization

1. Denhardt's hybridization solution was replaced by a fresh one and radioactively labelled telomere probe was added.
2. The gel was hybridized over night at 55 °C in a hybridization oven.

Membrane washing

1. The Denhardt's hybridization solution was discarded.
2. The gel was washed twice for 20 min at 55 °C with 4× SSC and twice for 20 min with 4× SSC and 0.1% SDS.
3. The gel was rinsed with 2× SSC and wrapped in a plastic foil.

Hybridization signal was detected. Under native conditions, only telomere G-overhangs were available for hybridization with the radioactively labelled telomere probe.

A.3 Denatured DNA rehybridization with a radioactively labelled telomere probe

1. Gel was denatured in a 0.6 M NaCl and 0.2 mM NaOH for 1 h at a room temperature.
2. The solution was replaced by a 1.5 M NaCl and 0.5 M Tris-HCl (pH 7.4), and the gel was neutralized for 1 at a room temperature.
3. Gel was rinsed with a sterile water for 30 min at a room temperature.
4. Gel was hybridized with a radioactively labelled telomere probe again according to **section A.2**.

A.4 Results

Despite of repeated experiments, no hybridization signals were detected (**Figure A.1**).

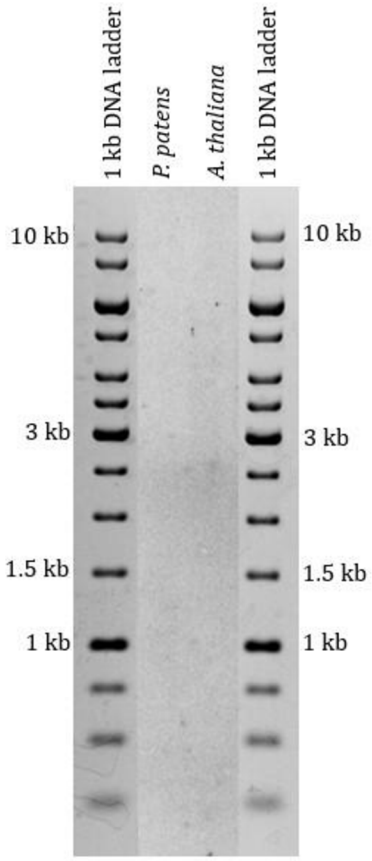

Figure A.1 In gel hybridization of DNA from *P. patens* wild-type and *A. thaliana* leaves digested by *MseI* with radioactively labelled PlTelC oligonucleotide.

Appendix B *Arabidopsis thaliana* cultivation

A. thaliana used in thesis in optimisations was cultivated on MS medium (Murashige-Skoog medium, pH 5.8; Duchefa Biochemie) diluted in a 1:1 ration with distilled water mixed with plant agar (final concentration 1% (w/v)). Before sowing, seeds were sterilised in 75% ethanol for 5 min and in 96% ethanol for 1 min. *A. thaliana* seeds after sowing undergo a vernalisation in a cold chamber (4 °C) for 2 days. Subsequently, seedlings were cultivated in a phytotron under short day conditions: 8 h light (illumination 100 $\mu mol \cdot m^{-2} \cdot s^{-1}$) 21 °C; 16 h darkness 19 °C.

DNA from 7-day-old seedlings was isolated same as from *P. patens* according to **section 7.2.3**. Telomerase extract for TRAP positive control was isolated as described in **section 7.2.18**. Protein concentration was measured using Bradford method (**section 7.2.19**) and diluted to final concentration 50 $ng \cdot \mu l^{-1}$.